BEUREN FELIPE BECHLIN

Slope-Driven Simulation and Visualization of Turbidite Channel Systems

Work presented in partial fulfillment of the requirements for the degree of Bachelor in Computer Engineering

Advisor: Prof. Dr. Manuel Menezes de Oliveira Neto

Porto Alegre
June 2021

UNIVERSIDADE FEDERAL DO RIO GRANDE DO SUL
Reitor: Prof. Carlos André Bulhões
Vice-Reitora: Profª. Patricia Pranke
Pró-Reitora de Ensino (Graduação e Pós-Graduação): Profª. Cíntia Inês Boll
Diretora do Instituto de Informática: Profª. Carla Maria Dal Sasso Freitas
Diretora da Escola de Engenharia: Profª. Carla Schwengber Ten Caten
Coordenador do Curso de Engenharia de Computação: Prof. Walter Fetter Lages
Bibliotecária-chefe do Instituto de Informática: Beatriz Regina Bastos Haro
Bibliotecária-chefe da Escola de Engenharia: Rosane Beatriz Allegretti Borges

ABSTRACT

Turbidite channel systems have a high potential as prominent petroleum reservoirs with significant economic value. The study of such systems is fundamental both to increase the success of petroleum reservoir discovery and to improve the recovery rate of hydrocarbons during the extraction process. Hence, simulation tools that explore hypotheses about the evolution of these channels have great value for the petroleum industry. Some previous works have been developed to characterize these depositional systems. However, they tend to focus on specific sections of the system instead of on a broader representation of the entire complex. We propose a novel parametric approach that relates the main system characteristics to the terrain slope underlying it, thus allowing us to obtain a larger variety of shapes and modeled structures. Our results demonstrate the adaptability of the proposed approach through simulations that reproduce formations similar to those found in schematics available in the literature. Hence, the proposed approach leads to a more flexible and general system simulation and visualization. Such a system can be a valuable tool for turbidite complex characterization and analysis. It has the potential to help geologists to interactively evaluate hypotheses and gain insights about the processes that resulted in existing turbidite formations. This should help these professionals to estimate the potential of these formations as promising hydrocarbon reservoirs.

Keywords: Turbidite channels. Meandering. Aggradational reservoir model. Rulebased modeling. Stratigraphic architecture.

RESUMO

Sistemas de canais turbidíticos são um importante tópico de estudo, visto que essas formações concentram grandes quantidades de hidrocarbonetos aprisionados e, portanto, representam grandes reservatórios de petróleo com elevado valor econômico. O estudo desses sistemas é fundamental tanto para aumentar a assertividade no encontro dos reservatórios como também para elevar a taxa de recuperação de hidrocarbonetos do processo de extração. Dessa maneira, simuladores que exploram o campo de hipóteses sobre a evolução desses canais são de grande valia para a indústria de petróleo. Alguns trabalhos têm sido desenvolvidos para a caracterização desses sistemas deposicionais, todavia esses trabalhos têm como foco seções específicas dos sistemas e não uma representação generalizada de todo o complexo. Nesse contexto, esse trabalho propõe uma abordagem paramétrica que relaciona as principais características do sistema com a declividade do terreno em que ele se encontra possibilitando assim uma maior variabilidade de formas e estruturas modeladas. Os resultados obtidos demonstraram uma grande adaptabilidade da abordagem proposta através de simulações que reproduzem formações como as encontradas nas interpretações esquemáticas disponíveis na literatura. Dessa maneira, o método proposto permite uma simulação e visualização mais generalizada do sistema se mostrando como uma ferramenta de grande valor para caracterização e análise de complexos turbidíticos. Portanto, a metodologia tem o potencial de ajudar geólogos a testar interativamente algumas hipóteses e compreender melhor os processos nas formações turbidíticas e ainda estimar o potencial desses complexos como reservatórios promissores de hidrocarbonetos.

Palavras-chave: Canais turbidíticos, Meandragem, Modelo de reservatório agradacional, Modelagem baseada em regras, Arquitetura estratigráfica.

LIST OF ABBREVIATIONS AND ACRONYMS

CLS   Channel Levee System

CLC   Channel Levee Complex

NTG   Net-to-gross

CAD   Computer Aided Designs

CLD   Centerline Distance

MD   Margin Distance

Z   Elevation

LIST OF FIGURES

LIST OF TABLES

CONTENTS

1 INTRODUCTION

Turbidite channel systems are a common type of sandstone deposit on the continental slope and have proven to be one of the most common types of hydrocarbon reservoirs found in deep ocean settings. The proper characterization of submarine channels in deep waters is a task with great value for the petroleum industry, considering the high cost involved in the discovery of these channels (WEIMER; PERKINS, 2000). Moreover, the characterization is a hard task taking into account that these submarine channels are longlived and large with a complex history of cut-and-fill and a corresponding multiscale hierarchy of erosional surfaces including even a broad variety of sediment scale (SYLVESTER; PIRMEZ; CANTELLI, 2011).

The problem complexity yields uncertainties for the oil recovery industry in many ways. These include, for instance, the volume of hydrocarbons at each place, and the facility scale needed for the most efficient hydrocarbon recovery. Thus, the use of simulation is highly valuable for reservoir modelers allowing them to explore different configurations, sequence of events, etc., thus reducing the uncertainties already mentioned in this challenging scenario. In recent years, a few approaches have been developed to study the channel evolution and architectures aiming at the description of the stratigraphic and morphologic structures resulting from turbidite depositional processes. However, most of these works focused on turbidite lobes: Abdelgawad et al. (2015) use a surface based modeling to simulate the deposition processes of turbidite lobes, and Zhang, Pan and Li (2020) review of progress in 3D modelling of turbidite lobes.

1.1 Contributions

This work proposes a novel approach for simulating turbidite channel systems on which the terrain slope is a fundamental part of the process. This method extends an existing simplified state-of-the-art model that can represent some geological formations but lacks extensibility for different scenarios, such as variable terrain slope profile, description of sediment composition, and multiple geological cycles. The approach mimics physical depositional and erosional processes in a fraction of the time spent in a physical model simulation.

The model proposed model uses a deterministic rule-based approach that incorporates parametric relations regarding channel properties such as width, depth, and the

topography where it lives. These relations are the key to broaden the use of the model since they can be adapted when required. Moreover, the addition of 3D visualizations and animations to the model allows easier and better exploration and understanding of the turbidite system behavior.

1.2 Thesis Structure

The remaining of this thesis is organized as follows: Chapter 2 (Turbidite Channel Systems) presents an overview of turbidite channels and their components, providing some background and context for this work. Chapter 3 (Related Works) reviews and discusses two important works used as references for this thesis. Chapter 4 presents our approach for simulating turbidite channel systems, describing the enhancements proposed to the current state-of-the-art method of (SYLVESTER, 2019). Chapter 5 presents some results obtained with the proposed simulation approach and compares them against data available in the literature. Finally, Chapter 6 presents some conclusions and directions for future work.

2 TURBIDITE CHANNEL SYSTEMS

This chapter provides the geological context for this work including the structure characteristics of turbiditic systems, related concepts, and the main phenomena involved in building and changing such systems.

Turbidite channel systems, also known as *submarine channel systems* or even *levee channel systems*, are geological formations that act primarily as a routing system for sediment into the ocean. They are located in the transition of the ocean shelf [1] and the basin floor [2]. Their architecture is both affected by erosion and deposition caused by submarine current flows, called *turbidity currents* which will be introduced in the Section 2.3, and other submarine mass movements. The whole transport system could stretch for hundreds of miles out into the abyssal plain and collectively contain hundreds of cubic feet of sediment (WANG, 2015).

Figure 2.1 – Generalized sediment-routing system illustration.
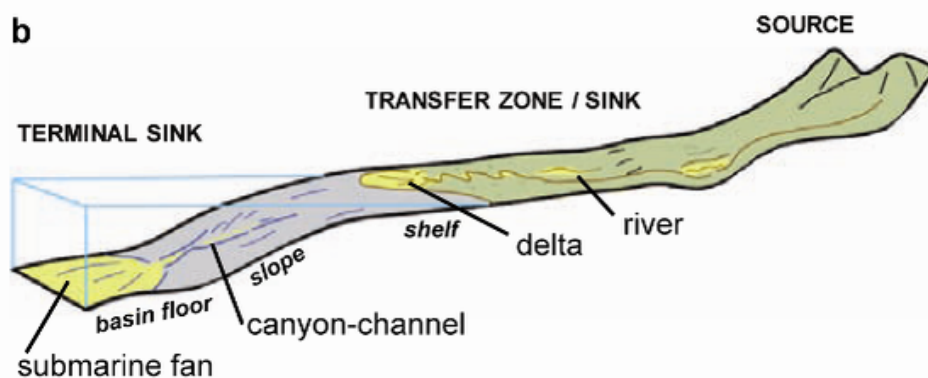
Source: (COVAULT, 2011)

Turbidite channels are not stationary in time, they tend to migrate, changing their course form, in a similar way as rivers. This migration is influenced by the gravity flow forces that act on the fluid causing different erosion rates on the channels' margins. Besides erosion, deposition is also a key factor in the migration process since the sediment tends to stick to the channel margins as well. The balance between these two factors determines the state of the channel at each moment, resulting in a continuous channel evolution throughout time.

---

[1] the edge of the continent that is submerged in relatively shallow water
[2] the lower part of the ocean basin, which is usually flat and adjacent to the continent

2.1 System Structures

In nature, these systems are quite variable depending on the specific area characteristics where it is located since the topography, rock, and sediment properties may vary from place to place. Nevertheless, the overall architecture remains the same and was described in (SPRAGUE et al., 2002). This architecture is characterized by the channel arrangement underneath the water that are also strongly influenced by the terrain slope, which indirectly quantify the sediment energy. The channels originate in sharp slopes in the form of *canyons* that progressively become shallower and wider until they end as *lobes*.

Figure 2.2 – Turbidite channel system illustration relating the systematic change in reservoir architecture down-slope.
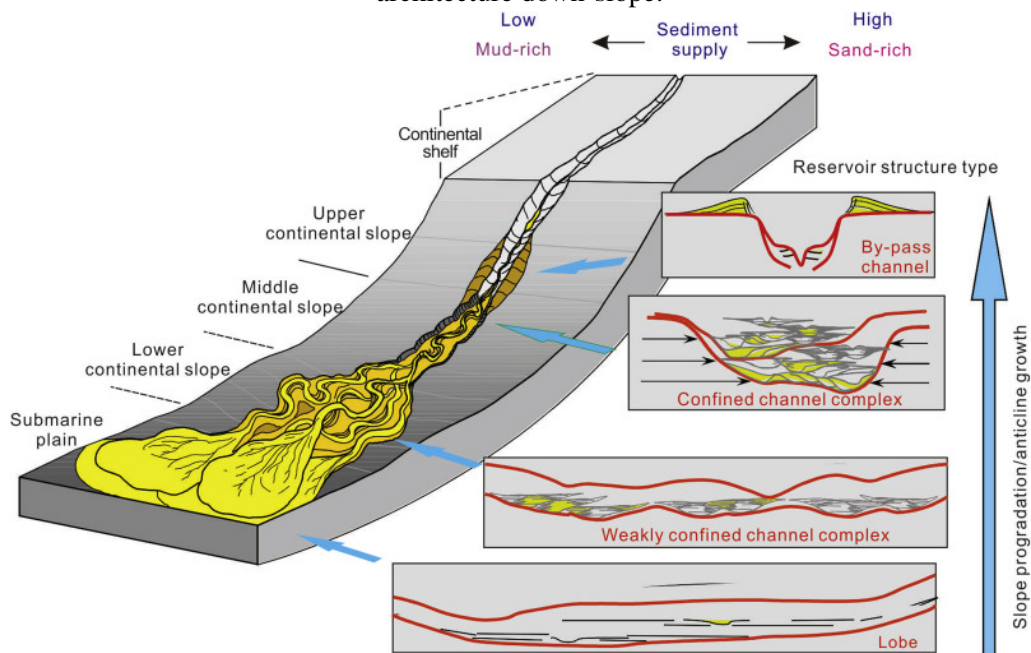
Source: (SPRAGUE et al., 2002)

2.1.1 Canyons

Submarine canyons are erosional V-shaped features very confined developed in steeper gradient slopes. These canyons are located in the transition from the ocean shelf, where in general low gradients are observed, and the continental slope (see Figure 2.2). These formations tend to present levee[3] sediment in their margins and lower migration

---

[3]the sediment that deposits in the channel's margins as dike or ridge confining the flux inside the channel

rates, thus are more straight compared to channels in middle and lower continental slopes (Figure 2.2). This is the most erosive part of the system, which leads to deep channels. In Figure 2.2 canyons are referred to as *by-pass channels*.

2.1.2 Confined Channels

Confined channels are also the product of strong erosional flows and present moderate migration rates. At this stage, the channels are U-shaped and erosional/levee confined. They tend to develop multiple complexes vertically stacked with a low aspect ratio i.e., a low ratio between the channel's width and the depth, which means more squared contained architectures. Due to migration and vertical stacking, caused by deposition, confined channels show great connectivity in both axes. The confined channels are shown in *middle continental slope* in Figure 2.2.

2.1.3 Weakly Confined Channels

Weakly confined channels are characterized by slight erosion and high migration rates. This environment presents shallow channels on which the slope is high enough to transport sediments down instead of local deposition, but not as high as necessary to develop confined channels. The resulting architecture has a high aspect ratio containing wide reservatories that are not densely connected compared to confined channels, but have good lateral and vertical continuity. Weakly confined channels in general have high net-to-gross (NTG) i.e., the fraction of reservoir volume occupied by hydrocarbon-bearing rocks, and are not levee confined. They are represented in Figure 2.2 in the *lower continental slope*.

2.1.4 Lobes

Lobes are formed in the final part of the system, located on the basin floor where the slope is very small or negligible, and having very high NTG terminal splays. Lobes are an important study topic in geology since they are reservoirs that have massive hydrocarbon potential and represent one of the most promising exploration targets for the hydrocarbon industry (ZHANG; PAN; LI, 2020). These structures present depositional

radial patterns and are feed by the channels preceding them. The lobe stacking pattern presents high lateral continuity but poor in the vertical continuity due to its depositional pattern. In general, these lobes are big structures that can even stack on top of each other. These structures are represented in Figure 2.1 as *submarine fans*, and in Figure 2.2 as *submarine plain*.

2.2 Meandering

The term *meandering* refers to a series of sinuous curves and bends of a watercourse as shown in Figure 2.3. This process is a central concern to geology and civil engineering since it has practical implications in land use, sediment budgets, and navigation (HOWARD; KNUTSON, 1984). The most recognized scenarios where it occurs are rivers, although it also happens in the submarine channels discussed in Section 2.1. The term *migration* refers to the spatial offsets in channel course which can be expressed in meters per year.

Figure 2.3 – Meandering process illustration highlighting erosion/deposition mechanics.
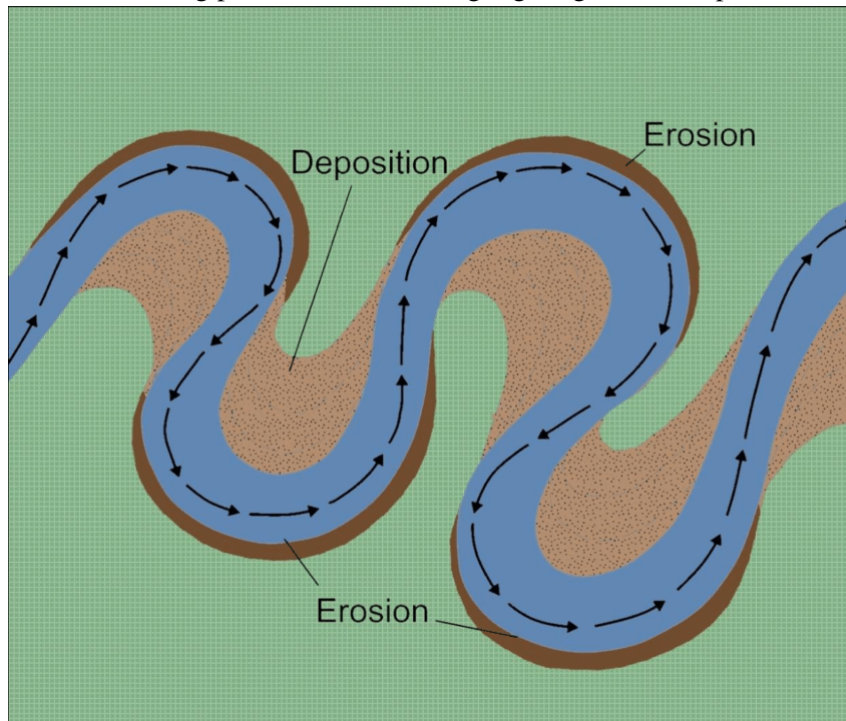
Source: (HIL, 2018)

The natural flow of a river, for example, introduces this kind of effect since any disturbance on the river course generates unstable sediment erosion and deposition. Even straight rivers tend towards this behavior as the result of any eventual punctual margin

erosion which unbalances the sediment flow and then is reinforced down-stream.

Figure 2.4 – Illustration highlighting the different flow velocities distribution in a straight cross section (A) compared to a bent cross section (B).
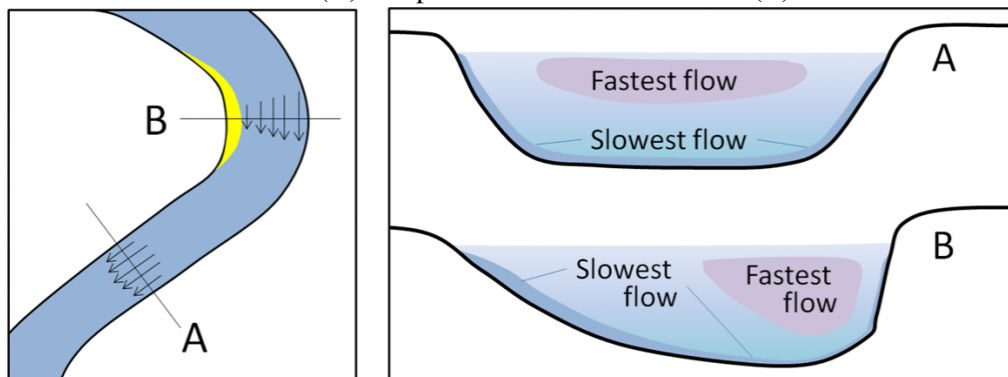
Source: (SURFACE..., 2020)

Figure 2.4 illustrates the main phenomenon behind this process: *fluid velocity profile*. Any moving mass body contains kinetic energy that is proportional to the square of its velocity. Thus, as the fluid develops a velocity profile instead of a single velocity for all particles, the energy is not equally distributed at the flow. Figure 2.4 establishes this difference in a bent cross-section in which the fastest flow is outside the bend and thus holds more energy and more erosion potential due to stronger frictional forces in the margin. The inside of the river bend, in contrast, contains slower flows which promote more deposition also due to friction with the margins, but instead of erosion, the sediment tends to stick to the margin since it does not hold enough energy to erode.

The migration trend towards curvier courses may lead to watercourse collision resulting in *cut offs*. In such a case, the course is adapted abandoning the bend. This often occurs in rivers, as shown in Figure 2.5, and is called *Oxbow Lakes*, but the same phenomenon also happens in turbidite channels.

2.3 Turbidity Current

Turbidity current is an underwater downslope flow driven uniquely by the weight of the sediment that it carries. It happens when water exceeds a sediment saturation that overtakes the frictional forces that were holding it into place. The result is a powerful wave of sediment that moves fast and dissipates quickly. Such flows are difficult to observe because they are rare and initiation mechanisms are still poorly understood and unpredictable (COVAULT, 2011).

Some recent studies discuss the turbidity current characteristics, such as (HEEREMA

Figure 2.5 – Satellite image of three oxbow lake formations illustrating the occurrence of cut offs in an pluvial system.
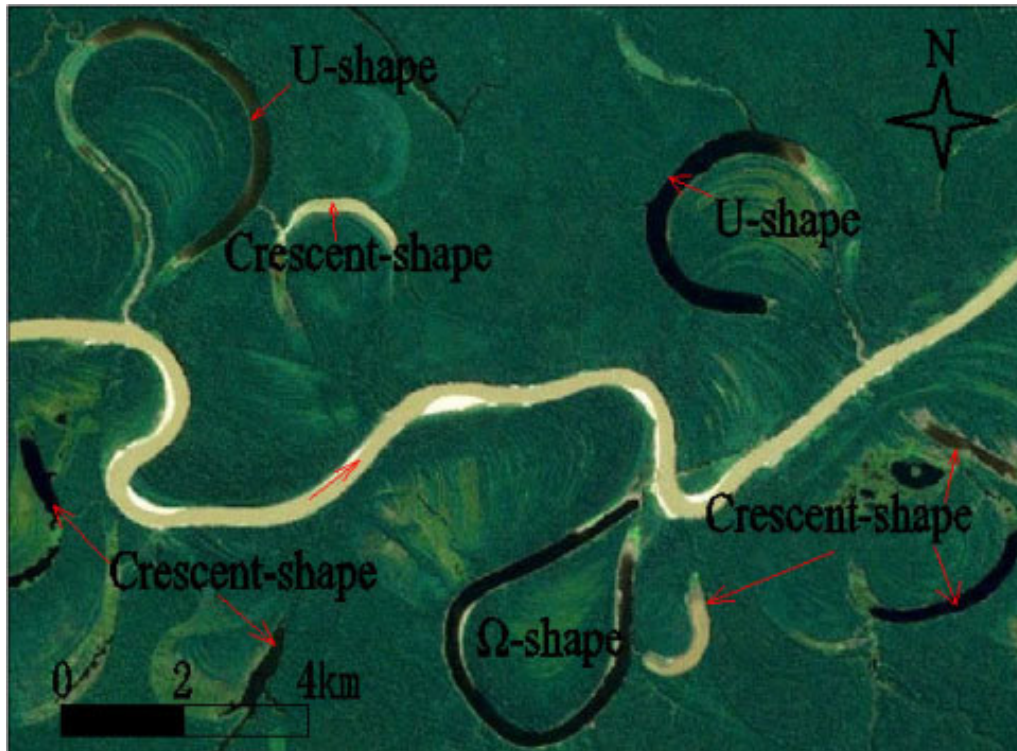
Source: (WANG et al., 2016)

Figure 2.6 – Turbidity current schematic representation.
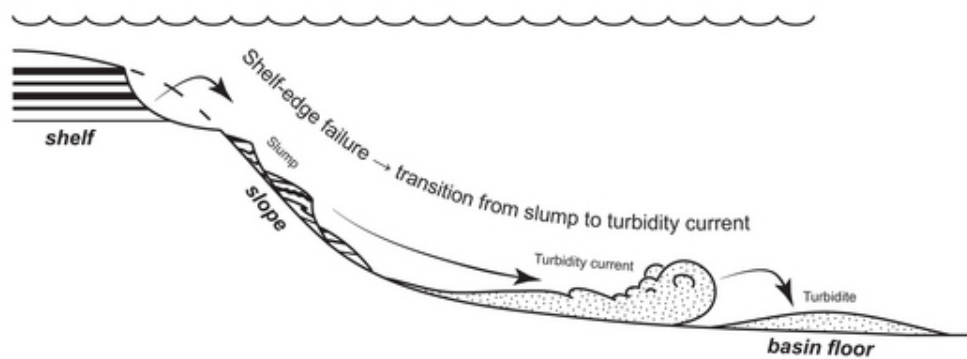
Source: (COVAULT, 2011)

et al., 2020), despite the notoriously difficult to monitor it in action. In this thesis, the focus is the overall properties that affect the turbite system architecture and fundamentally the sediment stacking behavior. Thus, flow evolution and its seabed interaction are the most important concepts in this context. Figure 2.7 presents a diagram for the turbidity current phases, which are described in the following subsections.

Figure 2.7 – Diagram exemplifying ignition, dissipation, and autosuspension phenomena in turbidity currents.
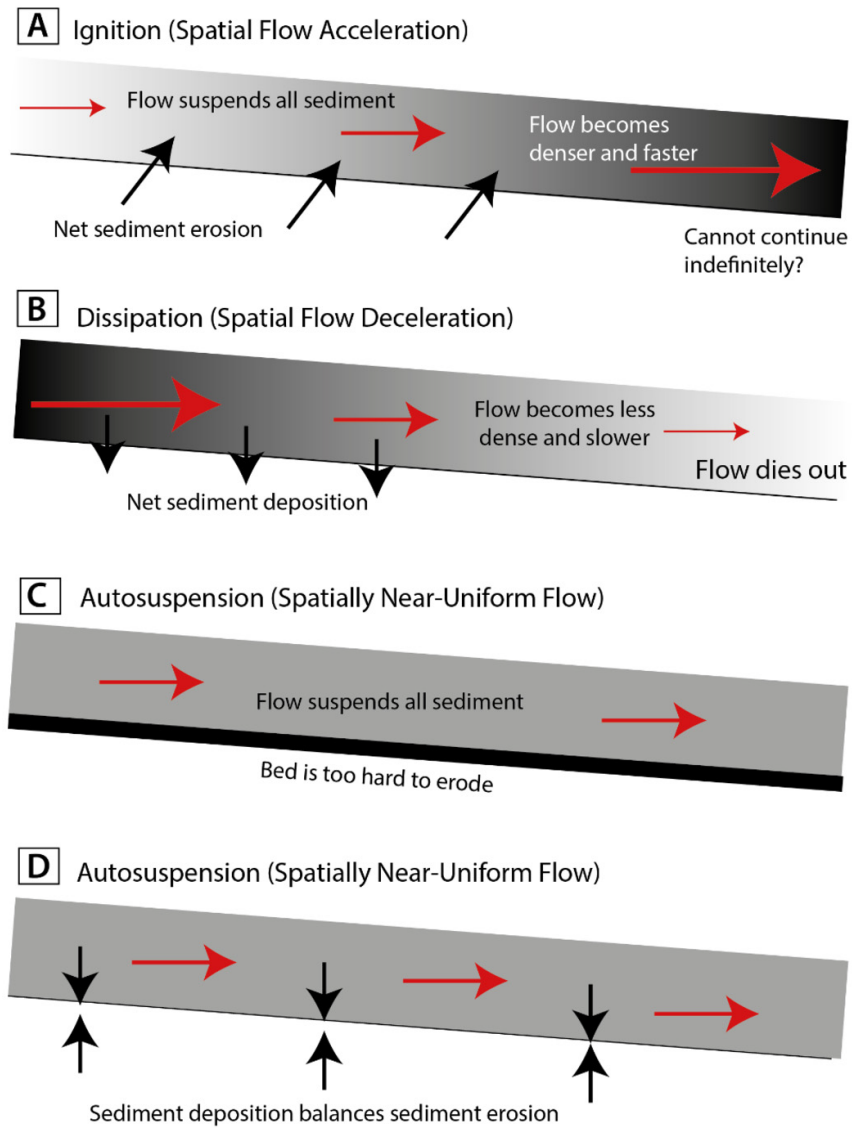
Source: (HEEREMA et al., 2020)

2.3.1 Ignition

All turbidity currents start in the ignition phase, in which the net sediment erosion increases the flow density causing increases in the velocity. However, this positive feedback cannot be sustained forever since these increases impact the flow regime or increase the friction.

2.3.2 Dissipation

The dissipation phase is the opposite, sediment is deposited causing a decrease in the flow density and thus flow velocity. In this case, the negative feedback rises until eventually, the flow dies affecting the runout distance.

2.3.3 Autosuspension

The auto suspension happens when the flow density and velocity remains constant. Two main scenarios exemplify this behavior, one when the bed is too hard to erode but the flow is powerful enough to carry all its sediment, and the other when net erosion is almost the same as the sediment deposition.

2.4 Equilibrium Profile

In the context of submarine channels, the equilibrium profile is the longitudinal profile on which the slope is kept in balance while the erosion and accommodation continue. The system tends toward this state since it is a low-energy configuration. In Figure 2.8, we can observe an example where the sections that lie below the profile have accommodation potential and the sections that lie above have a potential for erosion.

According to (KNELLER, 2003), turbidity currents are the determining factor of the equilibrium profile shape, although other agents are also important, such as traction, their contribution to the equilibrium profile development is minor.

Figure 2.8 – Schematic describing the equilibrium profile.
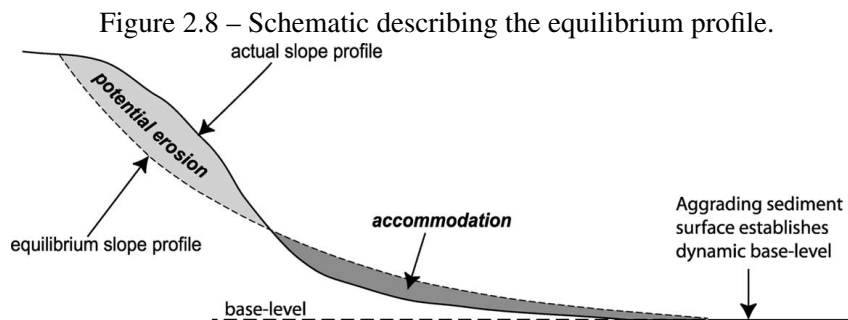
Source: (KNELLER, 2003)

2.5 Geological Events

Turbidite channel systems are sculpted primarily by the events already introduced in the previous sections. However, these environments are not static and changes in sea level or sediment density/granularity of the flows, for instance, may lead to completely different architectures. Thus, the literature identifies three main behaviors that are split into three categories.

Figure 2.9 – Schematic blocks of the turbidite system evolution and its filling deposits. (a) and (b) illustrate an incision cycle. (b) and (c), and (c) and (d) represent aggradation cycles.
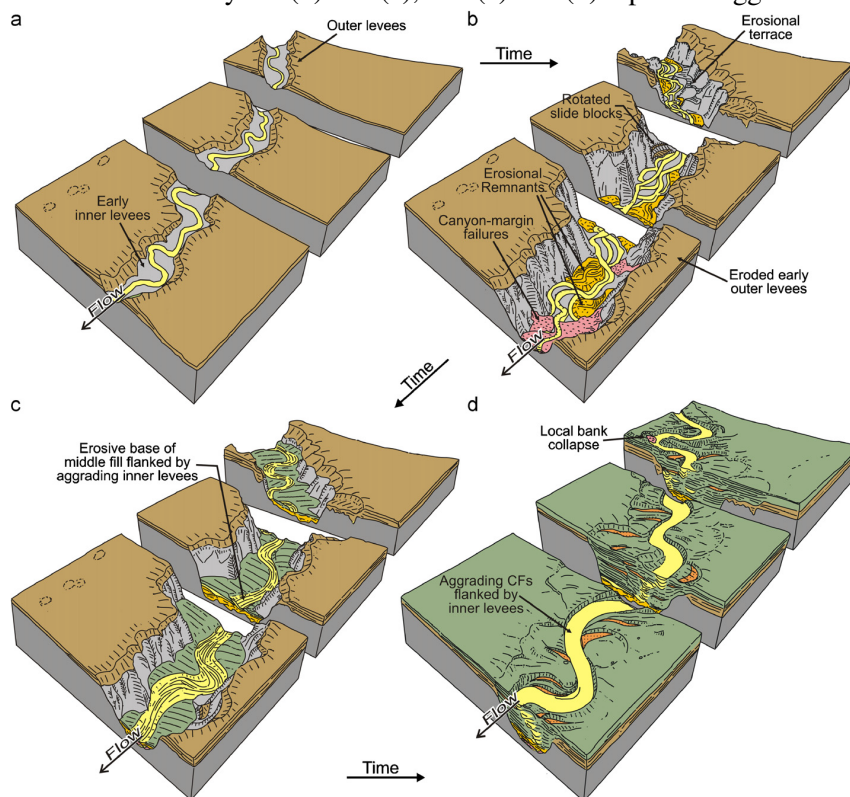
Source: (DEPTUCK et al., 2007)

2.5.1 Neutral

In this case, the slope is in equilibrium and, thus, there is no tendency to aggrade nor to erode. These channels still move but are constrained to migrate in the parallel plane to the equilibrium profile. Strong migrations also change the gradient configuration which can configure a phase of profile adjustments. The neutral cycle is characterized by the constancy of flow and sediment parameters.

2.5.2 Incision

The incision (or erosion) cycle is represented by the equilibrium profile flattening and by a decrease in sediment accommodation. This tendency occurs when the sediment flow is more abrasive, denser and usually sandier. The stability and the ability of such systems to achieve the equilibrium profile depends on the flow erosional potential compared to bed hardness, since as explained in Section 2.3, the current may stay in the auto suspension state if the bed cannot be eroded. The incised channels are often defined by the deposits that fill them, which is not completely related to the process that eroded these channels. Figure 2.9 (b) illustrates the incision cycle, with the channel eroding the substrate creating a confined valley.

2.5.3 Aggradation

The aggradation cycle is defined by the increased sediment accommodation which leads to a rise in the equilibrium profile. In general, caused by increases in sediment granularity size or by the reduction of flow density. The accommodation, as shown in Figure 2.9 (c) and (d), is most prominent at the base. However, when this happens the gradient at this section is decreased inducing more accommodation upslope resulting in a new equilibrium profile as mentioned.

2.6 Summary

This chapter introduced the different parts of the turbidite channel systems, the most common events that build and sculpt these channels, and how these environments evolve over time.

3 RELATED WORK

This chapter discusses two works that provide the basis for this proposed method. The first one provides the theoretical foundation for the first one, which in turn is extended by the technique presented in this thesis. The goal here is to explain their usability and assumptions, but a discussion of their implementations is important for understanding contribution of this thesis.

3.1 Meandering Simulation Approach

(HOWARD; KNUTSON, 1984) proposed a simulation approach for river meandering. Although it is a geophysical process, this method based on some assumptions and fluid mechanics concepts establishes the problem in a geometric formulation. This simulation approach makes the following assumptions:

1. Bank erodibility is constant;

2. Suspended sediment load is uniform downstream;

3. Migration is a continuous process that can be modeled in time steps that when summed cause pronounced migration;

4. Channel width is constant;

5. Flow and sediment input is statistically stationary.

Theses assumptions go towards the simplification of the channel by its course line and the remotion of any spatial dependency. An important concept of the proposed method is the nominal migration rate (R_0) which is defined by the channel curvature radius, as show in Figure 3.1, divided by the channel width (R/W) .

In the second approximation model, (HOWARD; KNUTSON, 1984) argue that the channel curvature and erosion rates are related not only locally but also to upstream channel geometry. This is mathematically represented by a weighting procedure of migration rates. Equation 3.1 is the general formulation for this approach, where R_0 is the actual migration rate, the R_1 is the adjusted migration, G is the weighting function, Ω and Γ are proportionality constants, and ξ is the distance measured from the centerline.

$$R_1 = \Omega R_0 + \Gamma \frac{\int_0^\infty R_0(s - \xi)G(\xi)d\xi}{\int_0^\infty G(\xi)d\xi} \tag{3.1}$$

Figure 3.1 – Visual definition of curvature of a generic curve.
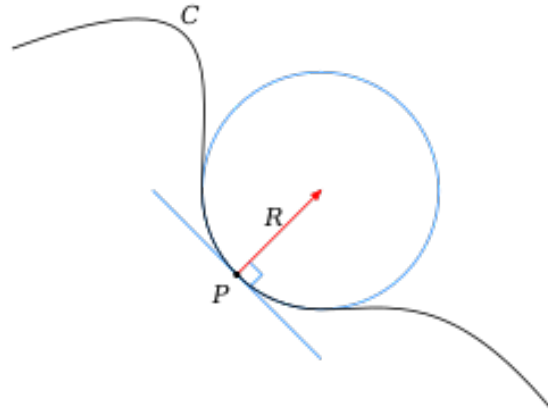
Source: (EMPERORHONEY, 2020)

The intuition behind this equation is that the migration one step forward is proportional to all present migrations upstreams weighted by how far they are apart. The work also proposes possible weighting functions G, which satisfy to the restriction that the integral from 0 to infinity is convergent i.e. results in a finite value. The exponential decay is the most common and used function in this context. Thus, G is defined as follows, where C_f is the friction coefficient, D is the channel depth, and k is a scaling parameter.

$$G(\xi) = e^{-\frac{2kC_f\xi}{D}} \tag{3.2}$$

These parameters come from the energy conservation principle, in which the energy spent in friction must be balanced by some other source as gravity in case of a slope. The derivation of this equation is based on the flow velocity response exposed to friction. Its details can be found in (HOWARD; KNUTSON, 1984).

After the calculation of the adjusted migration rate for the next step, the coordinates of the channel course should be updated. This process requires the time step width and the unitary normal vector at each point, which are then multiplied by the migration rate resulting in offsets for the channel course. The method requires an initial non-straight channel course, which is modified iteratively. Figure 3.2 shows some results from the authors, where the numbers mean the number of iterations.

3.2 Submarine Channel-Levee Evolution Model

Strongly inspired by the work of Howard and Knutson (1984), Sylvester, Pirmez and Cantelli (2011) proposed a 3D model for channel levee systems focusing on the strati-

Figure 3.2 – Meandering simulation results against the iteration number.
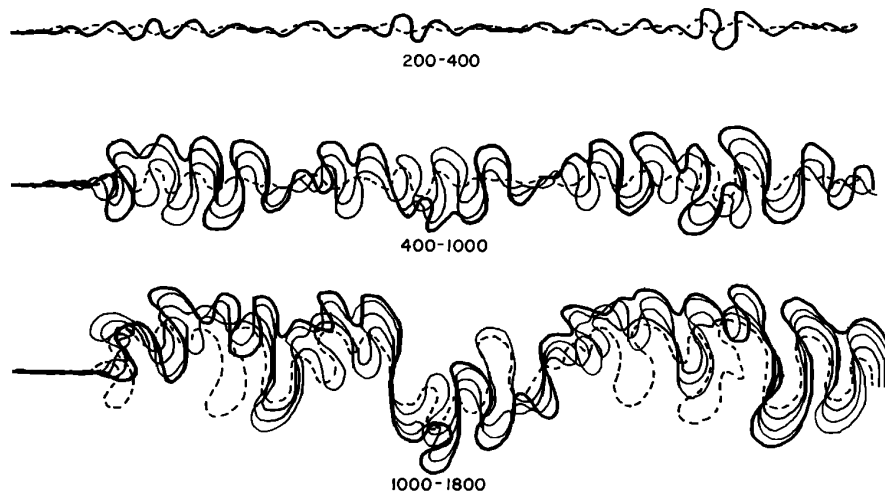
Source: Adapted from (HOWARD; KNUTSON, 1984)

graphic architecture. The method is based on the long sequence of cycles of cutt-and-fill of this system and makes the same assumptions that were discussed on the (HOWARD; KNUTSON, 1984) work. This model was made available through a Python package called *Meanderpy* (SYLVESTER, 2019).

Sylvester (2019) expands the migration from 2D to 3D introducing the channel elevation, which was omitted in (HOWARD; KNUTSON, 1984) and considering the gradient slope, since it is the most common power source in river flow. However, for rivers, this does not have a big impact due to the low ($< 5°$) slope where these systems are exposed. Thus, the introduction of the new dimension is associated with surface generation in space.

Sylvester (2019) factor the simulation process in two steps: channel meandering and surface generation. During the *meandering step*, the channel is represented by a set of points in 3D belonging to its course line. The simulation updates the positions of these points as well as the local parameters associated to the channel (e.g., depth, width, etc.). The surface *generation step* creates the stratigraphic representation, on which the resulting channels from the first part are extruded using a parabola to generate 3D surfaces. In the following subsections, this approach will be explained in more detail.

3.2.1 Meandering Step

This is fundamentally the migration step. As already mentioned, the user should provide an initial channel representation, mainly the channel centerline points, depth and

width, that serves as the system's initial state. Then, the migration algorithm is performed and periodically the resulting channel is saved as a new entry in a list called *channel belt*. The migration algorithm consists of:

1. One step migration using the Howard and Knutson's algorithm (HOWARD; KNUTSON, 1984) algorithm, which only affects the horizontal coordinates i.e. does not consider or change the elevation coordinate.

2. Search for possible sections in the imminence of crossing themselves and cut them out if any is found. The search for imminent crossings is performed by computing the Euclidean distance among every pair of points. A threshold distance between points along the centerline is established, which is the order of one to two times the channel width. Any distance above the threshold is not considered and set to infinity. Also, a metric window is defined to prevent the detection of subsequent points as crossings, in general between 20 to 25 points. Finally, the points with the minimum distance are linked removing the points in between them. The removed points result in oxbow lakes formations, as shown in Figure 2.5.

3. Resampling the course line to keep approximately the same distance between consecutive points, necessary for algorithm stability. The resampling is performed using spline fitting and resampling in evenly spaced intervals.

4. Simulate aggradation and incision cycles by adjusting the elevation coordinates of the simulation grid.

Figure 3.3 shows the system after the application of the steps listed above. The aggradation and incision cycles do not affect the view generated in this figure since it is a top view of the complex. Thus,we modified the *Meanderpy* package to capture the slope profile during the simulation.

Figure 3.4 shows the slope profiles associated to three different stages. The initial channel is created based on the terrain slope varying from -5° to 0°, which is perfectly smooth in Figure 3.4 since it is the input. After some iterations, the slope profile has changed due to incision and aggradation stages, resulting in instabilities which will be further discussed. However, the simulation of these cycles reproduces what is described in the literature, with the incision flattering the equilibrium profile and the aggradation rising the equilibrium profile and decreasing the slope in the low gradient part.

Sylvester warns about the instability of the slope profile in the Meanderpy package documentation (SYLVESTER, 2019) and this behavior is cumulative. Thus, the instabil-

Figure 3.3 – Meandering evolution sketch including identified entities.
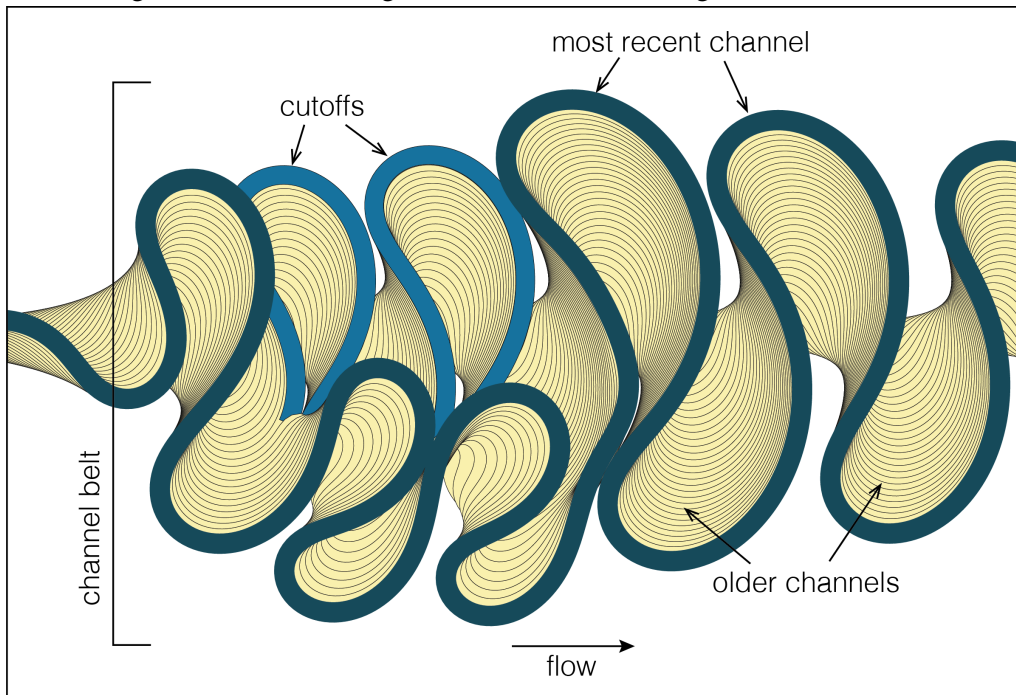
Source: (SYLVESTER, 2019)

Figure 3.4 – Slope profile in different stages of the simulation.
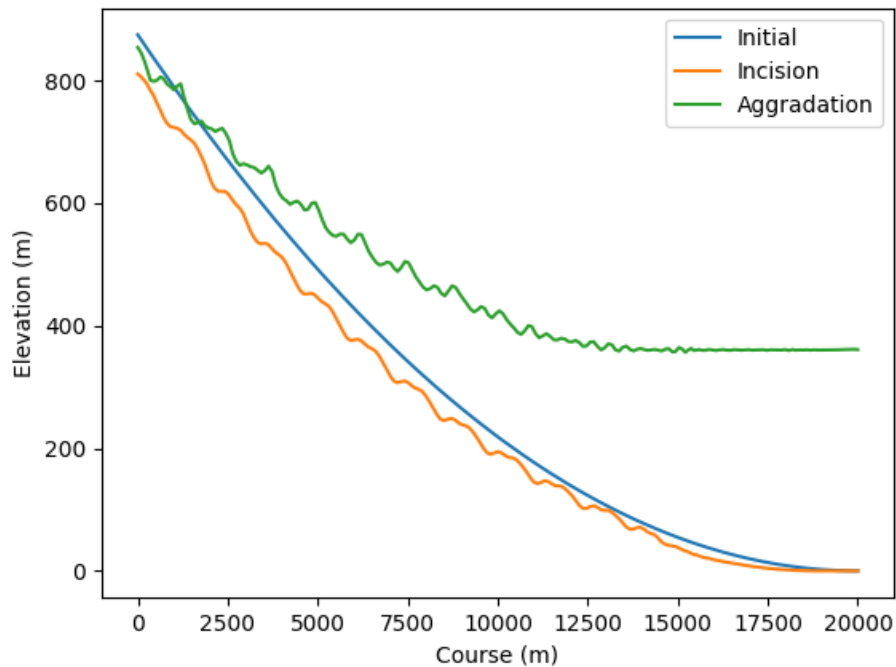
Source: Author

ity gets worse with more simulation iterations and can even become out of control causing algorithm to halt. This issue results from how the channel is represented and changed over time.

In the algorithm described earlier, the migration changes only horizontal coordinates preserving the previous elevation, which causes this instability since the elevation does not match the exact spot as before. This problem is even amplified by the migration algorithm nature that moves the points towards the bends, which is then corrected by the resampling step. However, the resampling step cannot deal with elevation artifacts since the elevation coordinate is already wrong when the spline fitting phase in the centerline takes place.

3.2.2 Surface Generation Step

In this step, we generate 3D representations for the simulated channels as a set of triangular meshes. Given the abstract representation of a channel (its centerline points, width, and depth), the surface generation step produces a set of heightmaps corresponding to the system's stratigraphy, which are then used to create the channel's 3D mesh representation, a stack of heightmaps representing the system stratigraphy. Note that the visualization module available in the Meanderpy package (SYLVESTER, 2019) only produces 2D views a channel, which consist cross-section plots of the system, as shown in Figure 3.5.

Figure 3.5 – Cross section image of an meandering simulation.

Source: (SYLVESTER, 2019)
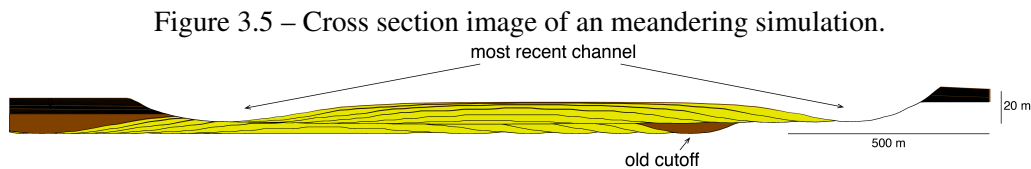
The generated heightmaps are based on a regular grid that is defined given a discretization factor. The discretization factor is in meters and corresponds to the grid step size. Thus, when this factor is small, the model will produce finer representation (mesh) at the cost of requiring more memory. This factor also affects the time required to generate the model.

The approach for generating the 3D mesh representation is incremental and based on images (2D maps containing information about channel course and margins). For each channel in the *Channel Belt*, a set of layers are computed on top of the surface of the last iteration. The first channel is used to extrapolate the initial surface, which is considered a constant slope terrain limiting the range of scenarios. The essential parts of this process are summarized and further discussed below:

1. Given the grid size and the grid step size, and the model boundaries, channel centerline is rasterized as a black-and-white (B&W) image 3.6;

2. The *morphology distance transform* operator is applied to the resulting image aiming at the creation of a distance map to the channel centerline, resulting in the centerline distance (CLD) map 3.7;

3. The channel elevation coordinates are also rasterized into a map, called Z map, of the same size as the CDL, but using linear interpolation 3.8;

4. The CDL and the Z maps and other information such as channel width are used to compute surfaces using parametric equations, such as Equation 3.3, which transforms the information of the maps into the corresponding surface, and is evaluated at each pixel resulting in the height of each grid cell;

5. The surfaces are combined with previously generated surfaces (i.e., surfaces from a previously simulated steps). The combination can be a sum/maximum of two surfaces, in the case of a depositional process, or the subtraction/minimum of surfaces, in the case of an erosional process.

Figure 3.6 – Channel centerline rasterized as a black and white image.

Source: Author

Figure 3.6 shows the channel course, also known as the channel's centerline, drawn as a black-and-white image. Naturally, the elevation coordinate is omitted. This image is only used for the centerline distance map creation.

The morphological distance transform is used to find, for each pixel in the binary image, the smallest distance to the centerline. This operation is defined for binary images in image processing and depends on the distance metric used. The chosen metric here is Euclidean distance since the goal is to find the length of the shortest line segment that links the pixel to another pixel belonging to the centerline. This transform is usually performed in pixel space but, when the dimensions represented by a pixel are known, it

Figure 3.7 – Centerline distance (CLD) map matrix rendered as an image. The color scale on the right indicates distances in meters.
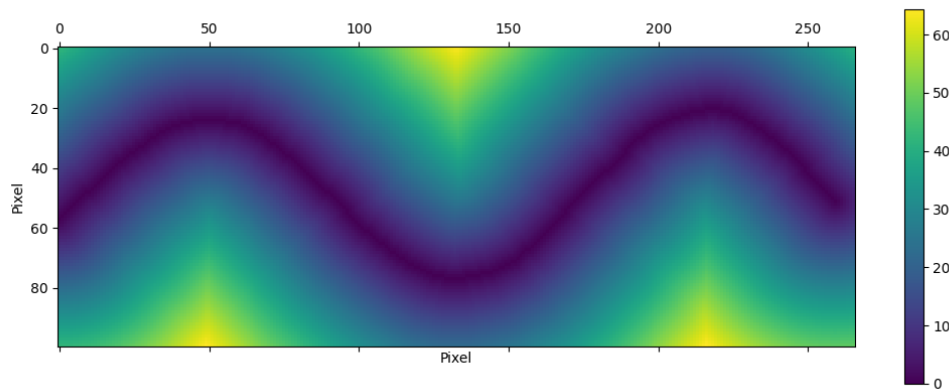
Source: Author

can transform directly to the problem space. The result of this operation is presented in Figure 3.7, resulting in a map of distances in meters to the channel course.

Figure 3.8 – Elevation map matrix rendered as an image. The color scale on the right indicates elevation in meters.
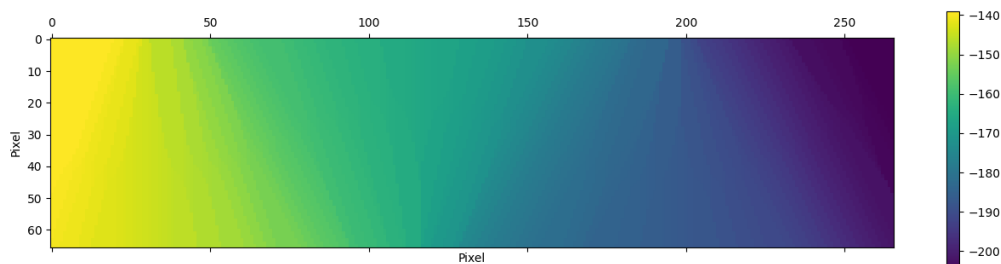
Source: Author

Considering that the information about the channel elevation is lost in the CLDmap a second map is created to represent such information. In this map, the elevation is linearly interpolated to fill all pixels in the image. Figure 3.8 shows the elevation map produced for the same channel shown in Figure 3.7, which corresponds to a terrain whose elevation varies from about 140 m to 210 m from left to right, corresponding to a slope of 1° along the way.

The centerline distance map and the elevation map combined with other constant parameters are then evaluated by the surface equation. For example, Equation 3.3 is a parabolic equation used to create an erosional S surface based on the channel profile. The term H corresponds to channel depth, W to channel width, cld_{map} to centerline distance map, and z_{map} to elevation map. Both cld_{map} and z_{map} are computed *pixelwise* and H, W

Figure 3.9 – Erosional surface matrix rendered as an image.
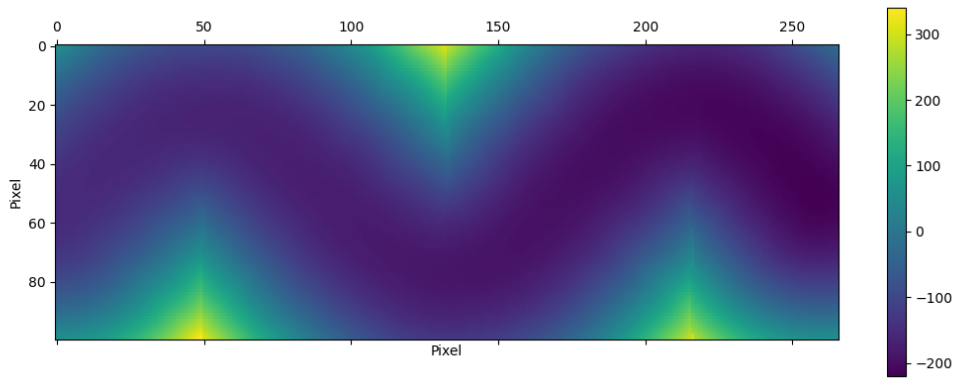
Source: Author

are constants. When the cld_{map} is zero, i.e., the point is on the centerline, the equation simplifies to $S = z_{map} - H$, which correspond to the minimal point and the channel's bottom. Moreover, when cld_{map} is equal to $\frac{W}{2}$, i.e., the point is on the channel's margin, this result in $S = z_{map}$, which corresponds to the current z level. For cld_{map} outside this interval the surface gets indefinitely high.

$$S = z_{map} + 4\frac{H}{W^2}(cld_{map} + 0.5W)(cld_{map} - 0.5W) \tag{3.3}$$

Figure 3.9 shows the resulting surface using the maps explained above and $H = 12, W = 200$. In the case of the erosional surface, the combination is given by the minimum operator between the current surface and the erosional one. Figure 3.10 shows a 3D plot with the top-most surface generated for the first iteration of the channel simulation process. This is the result of the initial terrain surface combined with the channel erosional surface, then combined with the sand deposition surface inside the channel and finally combined with levee deposition surface outside the channel. This process continues for each channel in the *Channel Belt* (i.e., each iteration of the simulation process), combining the surfaces and stacking the results. Once all surfaces have been processed, the result is a 3D matrix of heightmaps, which can be indexed for cross-section visualization.

3.2.3 Final Thoughts about Meanderpy

Although the method can represent a range of scenarios using different initial channels or/and different parameters, some limitations reduce its applicability to real scenarios. For instance, the channel width and depth as well as the channel slope must be

Figure 3.10 – Three dimensional visualization of the terrain and erosional surfaces combination.
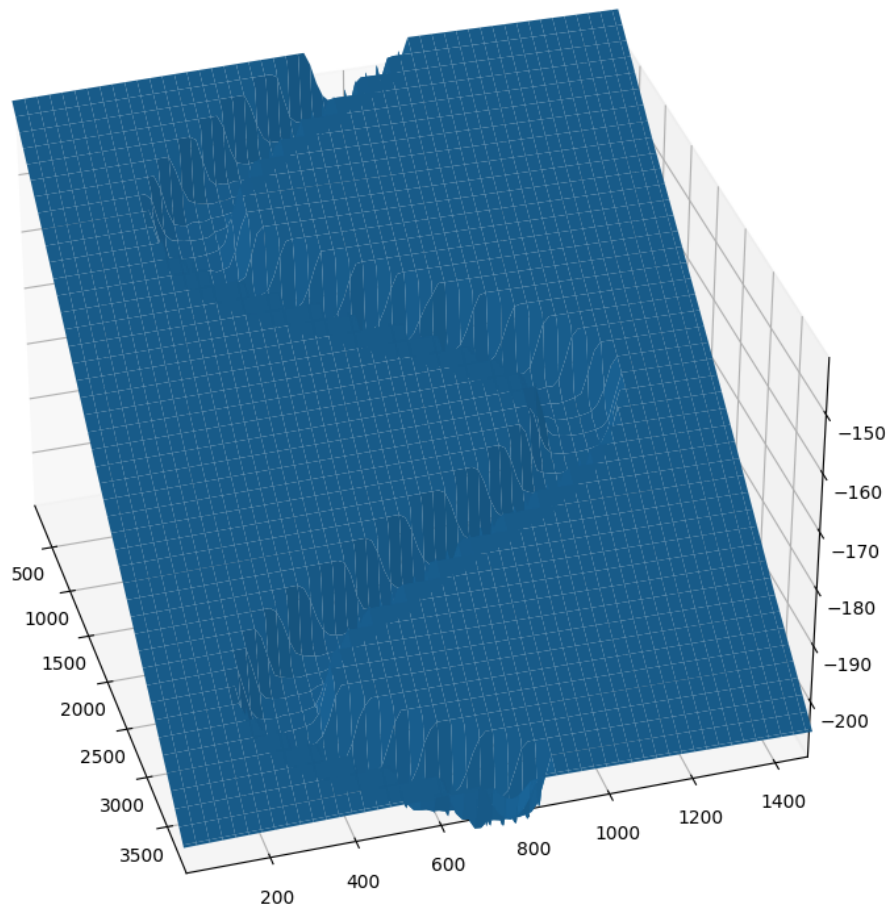
Source: Author

constant all along its course. However, as shown in Figure 2.2, the channel width and depth are expected to vary down-slope at the same pace that the terrain slope itself also changes producing different channel formations. Moreover, while the slope is a major determinant factor of channel formation, Meanderpy currently ignores its sign. Thus, given a certain slope magnitude, the results produced by its simulations will be same, regardless of the slope being uphill or downhill. Note that this is incorrect and is independent of the previously listed limiting assumptions.

Another issue is related to the possibility of describing different stages in the simulation. Currently in Meanderpy, all geological cycles (aggradation, incision, and lateral migration) must be executed in sequence with the same configuration. For example, the system cannot simulate a scenario with two (or more) consecutive aggradation (or incision) periods.

3.3 Summary

This chapter discussed the meandering simulation approach of Howard and Knutson (1984), highlighting its equations. It also introduced the approach by Sylvester (2019) for simulation of turbidite channel systems, explained its procedures, and discussed its limitations.

4 SLOPE-DRIVEN SIMULATION AND VISUALIZATION OF TURBIDITE CHANNEL SYSTEMS

This Chapter describes our simulation and visualization system for turbidite channels. Our simulation model is inspired by the works of Sylvester, Pirmez and Cantelli (2011), and of Howard and Knutson (1984). It extends Meanderpy, but unlike it, our system is completely parameterized by the local terrain slope. In this sense, it corrects the Meanderpy limitations listed in the end of the previous chapter, thus producing more plausible/realistic simulations and providing the user with additional flexibility over the simulation process. In addition, our visualization module allows for 3D interactive exploration of the simulated channels, given geologists an additional tool to explore their hypothesis about the series of events that might have generated existing channel systems.

The main assumption for this work is that the basin slope is fundamental and determinant for the system architecture, which leads to channels whose widths and depths can vary along their courses. This assumption is supported by the (SPRAGUE et al., 2002) on which reservoir architectures are classified in terms of slope propagation. Implementing our method requires changes equations, data structures, and maps are not equivalent anymore in comparison to the ones used in Meanderpy.

Another important contribution of our method is regarding the deposition surfaces. It models three different materials commonly found in submarine channels: silt, sand, and gravel. These materials represent different scales of granulometry and density. Moreover, the deposition mechanism was changed to use Gaussian profiles. Different plots were also implemented for best exploration of the channel systems, including 3D visualizations. The next sections detail these improvements and modifications.

4.1 System Overview

In summary, the simulation is performed in two main steps. The first is to define the *initial environment*, which consists of the basin profile and the 2D representation of the channel course (Figure 4.1). The second step is the definition of the *events*, which are queued and consumed sequentially. Thus, the effects of the events are cumulative. Given these inputs, the simulation process generates the 3D representation as shown in Figure 4.1.

Figure 4.1 – Default slope-width relation for any event.
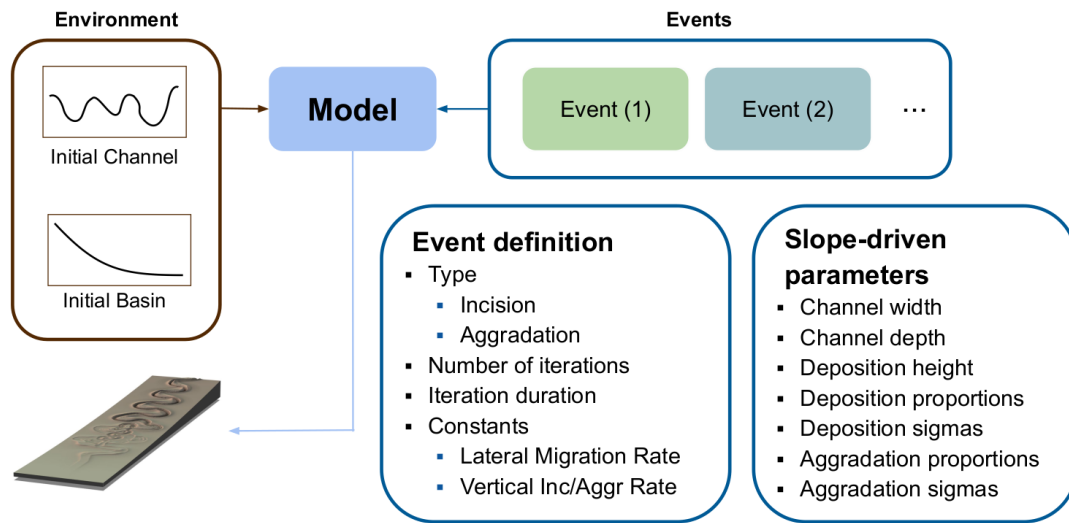
Source: Author

The events are defined by two set of parameters (Figure 4.1): *event definition* and *slope-driven*. The most important event-definition parameters are the event type (either incision or aggradation), the number of iterations, and the duration of each iteration expressed in years. The slope-driven and are explained in the following sections, but their meanings are presented bellow:

- Channel Width, and Depth: parameters used to determine the shape of the channel that is used to cut the terrain;

- Deposition Height, Proportions and Sigmas: parameters used in the deposition process that takes place after the channel cut step. One of the following sections is dedicated to explain how this process is performed;

- Aggradation Proportions, and Sigmas: parameters used in the aggradation process that is quite similar to the deposition process above. However, in contrast to the deposition, the aggradation only is performed when there is a elevation in the basin profile.

4.2 Parametric Modeling

At a first glance, a fixed relation can be established between slope and channel width/depth for a specific complex. However, as already discussed, different systems usually do not share the same characteristics. Thus, instead of fixed relation for all simulations, a parametric approach was chosen on which the reservoir modeler can easily

change and test with field data. In this approach, functions are the inputs to the simulation instead of constant parameters. For example, the default channel width relation is given by Equation 4.1, where s is the basin slope in degrees:

$$W(s) = 700e^{0.8s} + 95 \tag{4.1}$$

A set of model parameters is supplied in this way such as channel depth, deposition height, the proportion of each material in the deposition, the proportion of each material in the aggradation, the standard deviation of each material in the deposition/aggradation surrounding the channel's centerline, which will be covered later. All of them have already a default relation and only depend on basin slope.

These relations are empirical, derived from from drawings or tables that link a desired property to the basin slope. For instance, the values in Table 4.1 were obtained from geologists' drawings and were used to obtain Equation 4.1 through a fitting process. It is noticeable that the values in Table 4.1 have an exponential trend, and for this reason, an exponential function was chosen in the fitting process. Once we had defined which kind of equation best describes the data, we must found the parameter values associated with the given equation. For the case of Equation 4.1 we used the general form $Ae^{Bs} + C$, with parameters A, B and C. While different tools can perform this task, in this work we used the *curve_fit* function from the *scipy optimization* package, which uses the least squares to fit the data.

Table 4.1 – Established relation of channel width and basin slope obtained from geologist drawings.

slope(deg)	channel width (m)
-5°	100
-4°	125
-3°	150
-2°	250
-1°	400
0°	800

In the simulation process, the model parameters (e.g., channel width, depth, etc.) are locally evaluated based on the slope value, but only along the channel's course. Other parameters, such as the deposition and aggradation properties, are evaluated over the entire terrain (i.e., simulation grid). Thus, it is important to use smooth functions when defining model parameters to avoid discontinuity artifacts during the simulation.

4.3 Geological Event

Geological events are abstractions used to describe the simulation parameters and behavior. Thus, a system is characterized by its initial state and a list of events containing information about how the environment is at each moment. An event holds important information such as duration, type (whether incision or aggradation), relations introduced in the last section, and other simulation parameters.

This approach was designed to fill the gaps in Meanderpy concerning simulation flexibility discussed in Section 3.2.3. It is also intended to make the system more comprehensible, since the events are self-contained and can be studied and tuned apart from the simulation. To improve the user's understanding of the simulation process, one can examine all relations, as is shown in Appendix A - Figure A.1, associated to an event in the slope simulation interval, helping the geologist to geologist how the parameters are affecting the system.

For example, Figure 4.2 is the plot of the relation established in Equation 4.1, which is the default channel width relation for any event. In our system, the user can define any function $f(slope)$ describing the channel's width, depth, deposition/aggradation proportions, etc., as a function of the channel's slope.

Figure 4.2 – Default slope-width relation for any event.
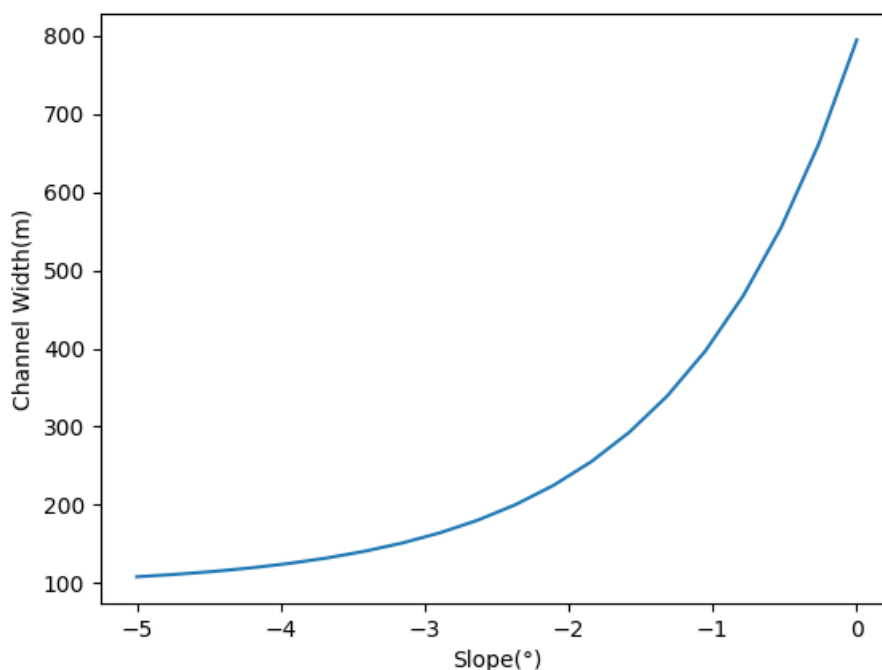
Source: Author

4.4 Basin Representation

Due to the slope profile instabilities discussed in Section 3.2.1, a different approach was introduced for the channel representation. In Meanderpy (SYLVESTER, 2019), the channels were the only data structure holding the system state in the meandering step. However, the elevation coordinates suffer from information degradation in this minimalist representation. Thus, present the basin in a distinct structure, which is responsible to determine the channel elevation.

The proposed basin consists of points in 2D that represent the side profile of the terrain similar to the one shown in Figure 2.8. Such a proposal assumes that the basin only changes in the forward direction and not laterally, but provides a good approximation in most places. This limitation is also observed in the (SYLVESTER; PIRMEZ; CANTELLI, 2011) method. Figure 4.3 shows the basin profile in three different moments during the migration step: the input basin, the basin after an incision event, and the final basin after an aggradation event. In this figure, the profiles are smooth and do not present the instabilities as in Figure 3.4.

Figure 4.3 – Basin profile plot of a two-event simulation: first an incision event and then an aggradation event, showing the cumulative effects on the basin profile.
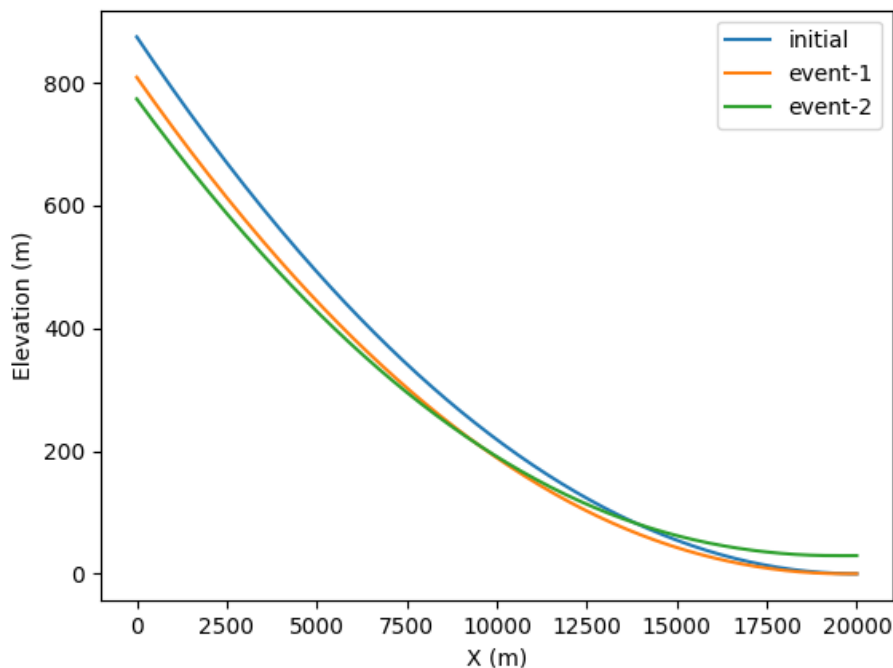
Source: Author

4.5 Meandering Step Adaptations

Channels with variable width and depth require changes in both (HOWARD; KNUTSON, 1984) method and (SYLVESTER, 2019) model. Some of the changes are straightforward in the sense that they do not impact the physics of the problem while others require changes in equations to represent this new scenario.

4.5.1 Channel Structure

Channels are still represented by a set of equally spaced centerline points, but in our system, the channel's width and depth at each point are also saved. This has implications in the channel reconstruction since the margins are not easily computed as before. To compute the channel margins we use *offset curves*(PATRIKALAKIS, 2003) in our parametric formulation. Offset curves are used in CAD applications in general. The method finds the normal vector to the curve which can then be multiplied by a displacement factor, as illustrated in Figure 4.4.

Figure 4.4 – Visual definition of general offset curves.
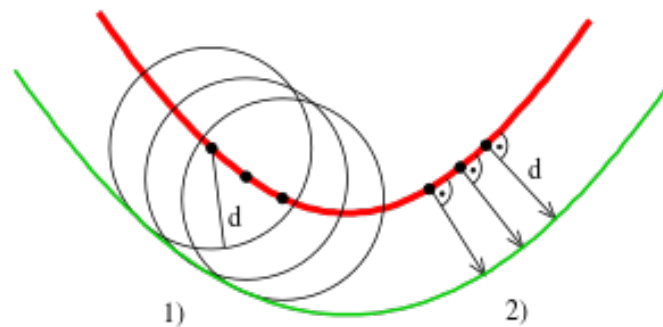
Source: (AG2GAEH, 2015)

Hence, each margin can be generated using the displacement factor as half-width at each centerline point. Figure 4.5 shows the method in action for a single channel with varying widths.

4.5.2 Cutoffs

The cutoff algorithm that allows the channel to take shortcuts while also creating oxbow lakes (Figure 2.5) must be also modified since it is based on a fixed distance

Figure 4.5 – Channel representation highlighting its variable width.
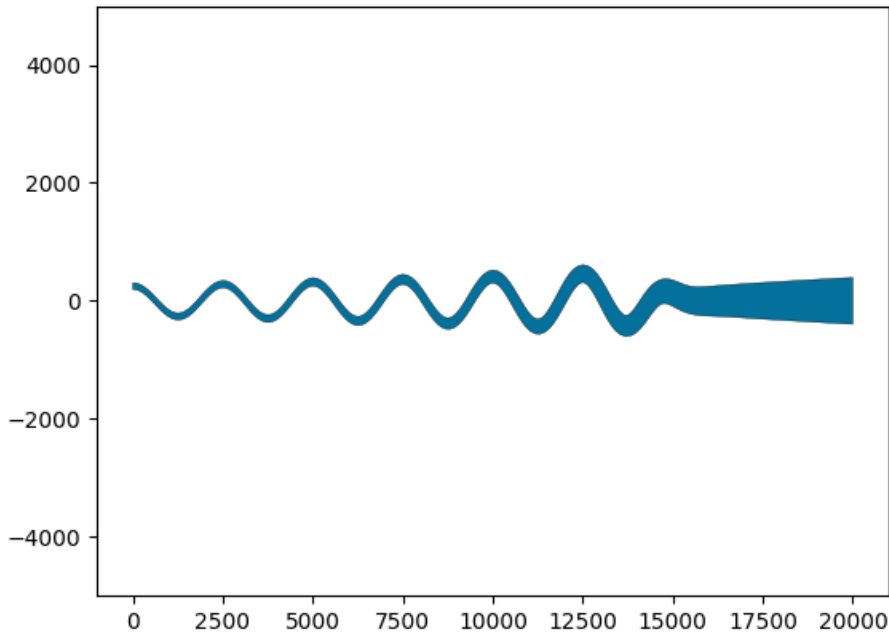
Source: Author

threshold using the channel centerline. This threshold distance should take into account the channel width since the distances are computed from the centerline and not from the margin. The proposed solution relies on the same algorithm of fixed distances but performed at each margin, removing the dependency to the variable channel width.

Moreover, a new algorithm for cutoffs is proposed to deal with artifacts in the sections of high migration rates. The migration rate depends linearly on the channel width. This amplitude is also reflected in the nominal migration producing anomalies that are amplified after a set of iterations. Figure 4.6 illustrates the occurrence of these artifacts.

To avoid these artifacts, we present a new cutoff algorithm is based on curvature $k = \frac{1}{R}$, where R is the local radius of curvature (Figure 3.1), and halfwidth $\frac{W}{2}$. Multiplying both terms get the dimensionless curvature $\frac{W}{2R}$, on which reveals two main scenarios: a dimensionless curvature value bigger than one ($R <= \frac{W}{2}$) indicates that the curvature is so steep that the channel with width W is not feasible; a dimensionless curvature value smaller than one ($R > \frac{W}{2}$), which makes the channel width feasible.

Hence, the new algorithms search for sections that the dimensionless curvature is greater than one. When such a section is found the algorithm cuts similarly as a normal cutoff, removing a set of points. The number of points removed is determined by the

Figure 4.6 – Channel belt plot showing artifacts caused by high migration associated with large channel width.
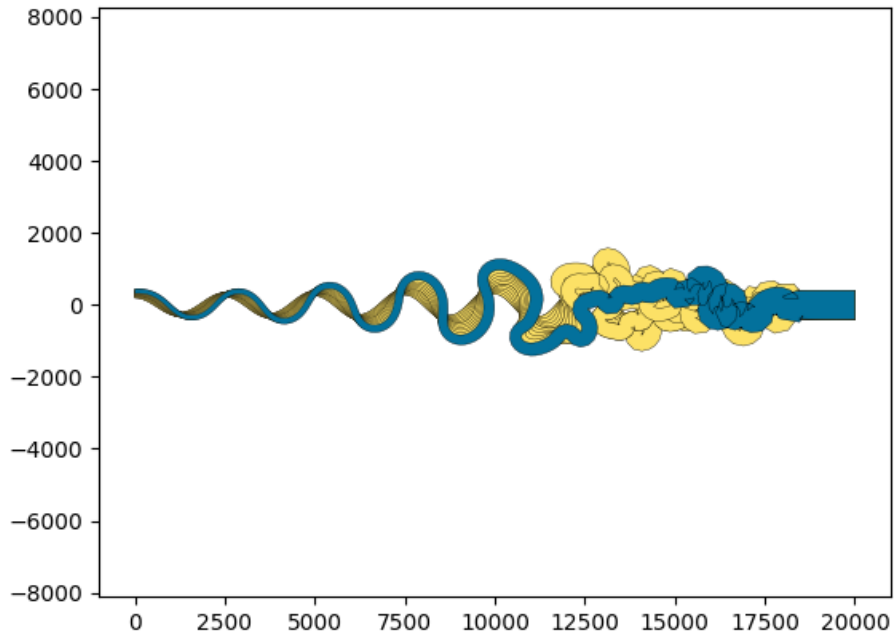
Source: Author

Figure 4.7 – Channel belt plot with no artifact after the new cutoff algorithm.
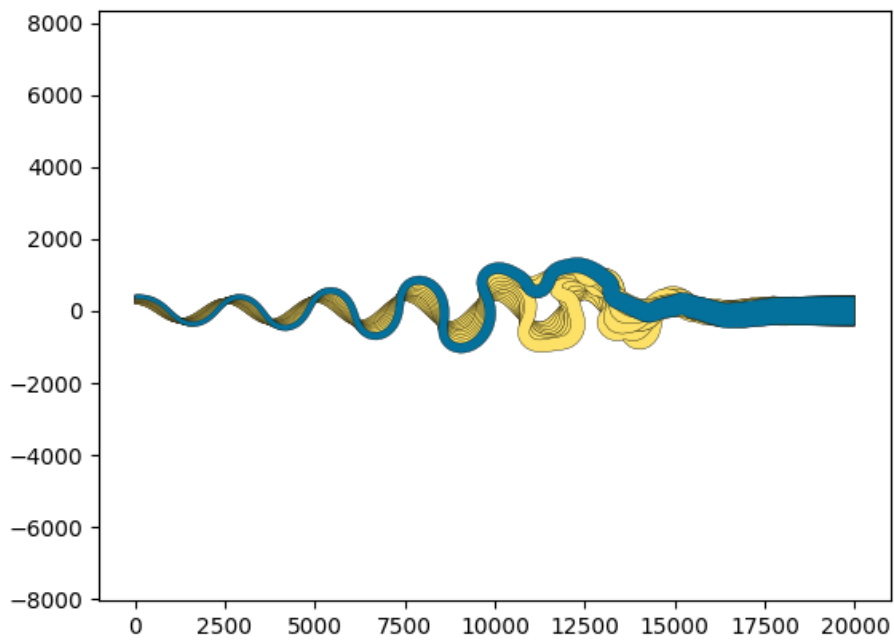
Source: Author

cutoff length, which was determined empirically to 1500 meters. Figures 4.7 presents the same simulation as Figure 4.6, however, both cutoff algorithms were used.

4.5.3 Migration Normalization

The (HOWARD; KNUTSON, 1984) work was developed having in mind a fluvial channel system away from the source and mouth. In this river section, the conditions are more stationary which allows the description by the overall behavior. However, turbite channel systems tend to be shorter than fluvial systems and present source (canyons) and mouth (lobes) relatively close to each other. Thus, the migration equation must be modified in some way that allows the usage all channel-long.

The equations proposed by (HOWARD; KNUTSON, 1984) make the assumption that a channel has a constant cross-section and is completely confined, i.e., it has constant width, depth, and no fluid spilling. This is important since the fluid profile velocity is highly related to the area it is confined to and friction is proportional to fluid velocity. As discussed in Section 3.1, the energy loss is supposed to be balanced by the slope in a way that the flow velocity remains constant. However, this is not the case in the turbidite system, since the turbiditic current eventually stops downslope. This phenomenon happens near lobes on which the channel is wide and shallow, thus being more depositional than erosional.

We propose a new normalization factor for the normalized migration rate computation, apart from the already existent ones, to model specifically the energy loss. This factor is based on an observation about the channel area that naturally tends to zero downslope, which is the same tendency of the channel migration. The channel cross-section area is approximated by a rectangle with base W and depth D for simplicity.

$$N_i = \frac{W_i D_i}{\lceil WD \rceil} \tag{4.2}$$

Looking in the perspective of the Continuity Equation $A_1 V_1 = A_2 V_2$ (SMITS, 1997), where sections with smaller areas the fluid should have more average velocity which is the opposite of what is observed in the channel system environment. However, the Continuity Equation describes an environment of energy preservation and fluid confinement which do not apply for turbidite channel systems. As this system has complex interactions with its environment, a simulation based on fluid-mechanics relations would

be computationally more expensive and require more data and boundary conditions.

The intuition the normalization factor shown in Equation 4.2 is that the cross-section area is indicative of fluid mass and the mass is responsible for the erosion. Thus in sections with larger areas more migration is observed compared to the ones with smaller areas. This is particularly true in this scenario where there are energy loss and fluid spilling on which the Continuity Equation is not respected. Note that this factor would not affect the channels described by Howard since the constant cross-section area would lead to a factor of one all along the channel.

4.6 Surface Step Adaptations

In the surface generation step, some changes were also necessary to support the channel modifications. Moreover, the deposition surfaces were changed to be more physically based and to give more control to the modeler/geologist.

4.6.1 Map Construction

The approach used to generate the erosional surface defined in Equation 3.3 does not support channels with variable width. To handle this situation, we introduce a new map that relates each pixel to its closer channel width that is called the *half-width* (HW) map. This map is computed using the original CLD map combined with another new map called *margin distance* (MD) map. The MD map generation follows the same steps as the CLD map, but instead of the centerline, the channel margins are drawn in B&W. Since the distance transform finds the closest pixel, the generated distance map considers the closest margin in all places.

The proposed method to compute the channel width in any place is illustrated in Figure 4.8, where D_{cl} is the distance to the centerline and D_m is the distance to the margin. Notice that the maps are displayed in the same image only for visualization convenience, since they are generated separately.

As shown in Figure 4.8, there are two different cases when estimating channel width: the pixel is inside the channel, or the pixel is outside the channel. In case the pixel is inside the channel, the half-width channel is determined by $WD = D_{cl} + D_m$. If the pixel is outside, however, then it is determined by $WD = D_{cl} - D_m$. To know if a

Figure 4.8 – Illustration describing how the half-width is computed based on the centerline and margin distance.
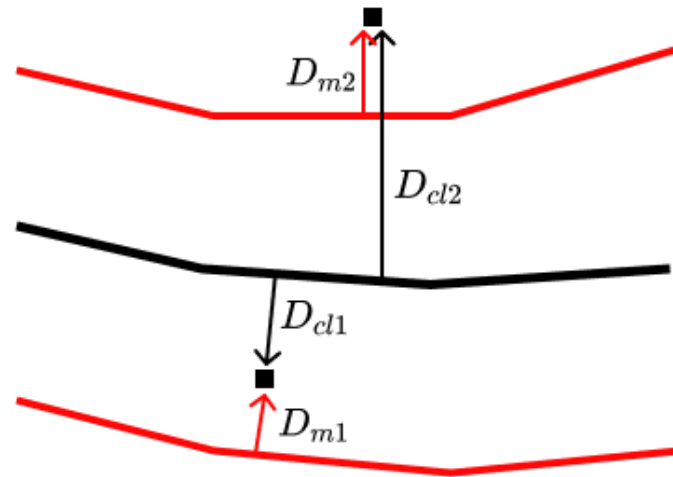
Source: Author

pixel is inside or outside the channel another intermediate B&W image is created filling the interior of the channel with white polygons against a black background. Then, the comparison is reduced to test if the pixel is black or white. Figure 4.9 shows the resulting HW map for a simulation.

Figure 4.9 – Half width map matrix rendered as an image.
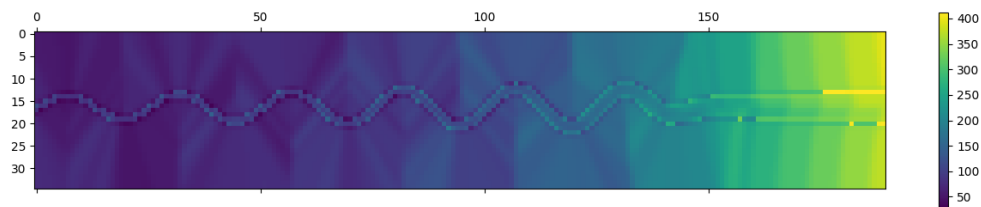
Source: Author

Once the map is computed, one can create the surfaces that simulate the incision and aggradation processes. For instance, Equation 4.3 creates the erosional surface in a parabolic profile, which is used to cut/excavate the channel in the current basin. In this equation, z_{map} represents the current z level of the basin, and cd_{map} the channel depth at each location which multiplies the terms that creates the parabolic formation. Moreover, we can observe in Equation 4.3 that when cld_{map} is zero, i.e. the point is on the channel's centerline, the result is $z_{map} - cd_{map}$ which is the lowest point that the surface can reach since it is the channel's bottom. This equation is also unbounded, as we can see in Figure 3.9, on which the surface gets higher far from the centerline.

$$S = z_{map} + cd_{map}[(\frac{cld_{map}}{hw_{map}})^2 - 1]$$ (4.3)

Figure 4.10 – Three dimensional rendering of the erosional surface clamped in elevation 1000 meters for better visualization.
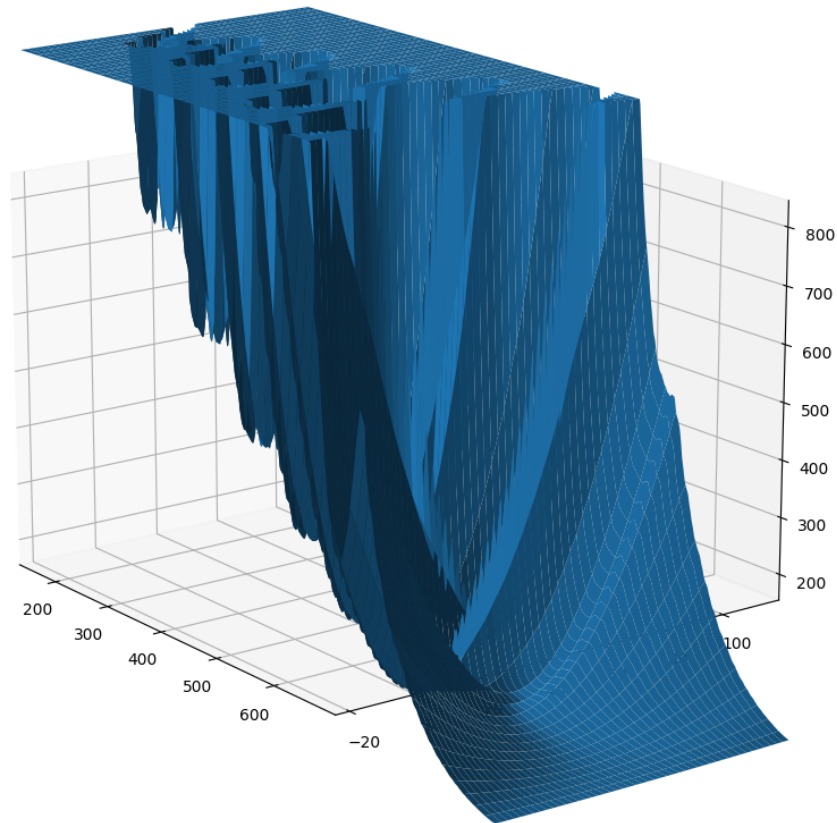
Source: Author

4.6.2 Depositional Surface Generation

The proposed method uses gravel, sand, and silt materials to simulate the depositional process. In the literature, these materials have finer subdivisions that were not taken into account. These three materials, however, are the most easily identifiable in the systems which helps with the simulation parametrization for the modeler. Moreover, the cost of the simulation depends linearly on the number of materials (layers) used and on the number of iterations. Hence, the usage of a limited set of materials allows long simulations.

Table 4.2 shows the granulometry scale of the used materials and a qualitative

Table 4.2 – Deposition materials and their granularity scale.

	scale (mm)	density
Gravel	4,00 - 2,00	high
Sand	2,00 - 0,06	medium
Silt	< 0,06	low

density scale that supports the proposed layer stacking order. Denser materials tend to deposit deeper in decantation, thus the deposition order is always gravel (orange), sand (yellow), and silt (brown).

The method is based on a cut-and-fill strategy which is described in (DEPTUCK et al., 2007) as the predominant factor, summed to channel migration, for the system geometry. Hence, the cutting phase is performed by the erosional surface as shown in Figure 4.10. The filling phase is based on the following assumptions and simplifications:

- The materials have boundary layers perfectly defined, even though the materials are mixed in the turbiditic current. This condition is naturally reached after a while due to density variability.

- The material tends to be deposited inside the channel since it is the lowest energy state.

- The deposition of each material follows a scaled Gaussian distribution centered in the channel centerline. This is a simplification for the deposition process which allows a good and simple parametrization.

Figure 4.11 shows a schematic illustrating the elements of the Gaussian depositional process and the parameters that emerge from it. Notice that in this schema the coordinates are normalized by the channel width, thus the only parameter that still has units of meters is the dep_{height} that is the deposition height, i.e., the height of all materials summed together. This normalization is important since the width is variable downslope. Hence, the standard deviations, which measure how close the material is deposited around the centerline, are given in this normalized space.

Instead of the definition of each deposition height separately, the approach establishes the material proportions of the total deposition height. The deposition height is measured in the center of the channel where each material has the highest deposition. The result of the method is represented in Figure 4.12, which shows a cross-section image generated using a few iterations.

Moreover, in case of aggradation events an additional depositional process is required since the channel's elevation rises and this difference must be filled up with de-

Figure 4.11 – Schematic representation of the Gaussian deposition approach of gravel, sand, and silt.

Source: Author

posits. For these events, our system uses a Gaussian approach similar to the one described above, whose standard deviations, referred to as $aggr_{sigmas}$, are bigger in order to create flatter deposits layers that overcome the current channel's margin. This behaviour can be visualized in Figure 2.9-(c). There, the channel is filled up with deposits in yellow that correspond to the deposition process. Also, the basin cavity, formed by early incision channels, is filled with deposits in green that correspond to this aggradation depositional process. Thus, the complete amount of deposited material in our channel simulator is the sum of the channel deposition and the aggradation deposition. The aggradation deposition is zero in incision events.

4.6.3 Visualization

The cross-section images are quite important to describe in detail the observed formations in nature. However, only looking cross sections of the channels is hard to understand the complete system behavior. Therefore, a 3D visualization module was implemented using R and a specific library for map rendering. Since our system was written in Python, the multi-layer 3D model of the channel system must be exported

Figure 4.12 – Cross-sectional plot illustrating the Gaussian depositional approach.
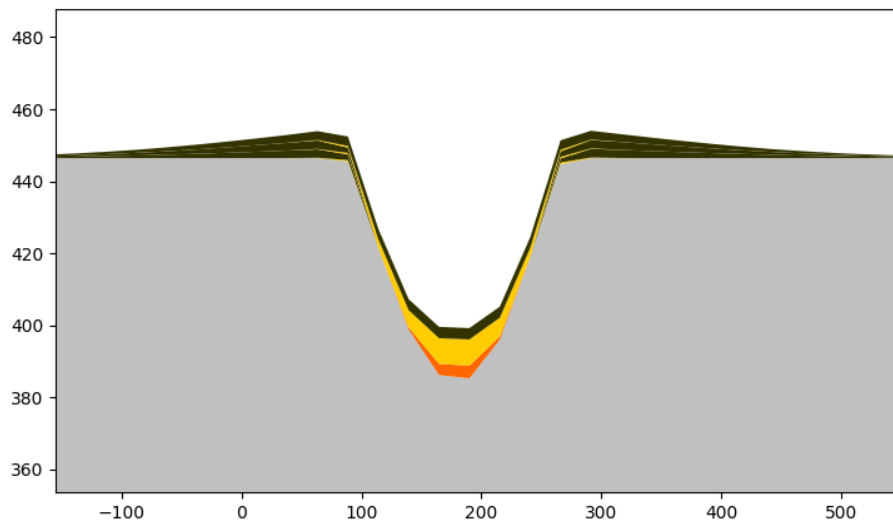
Source: Author

after the simulation, and then it can be imported into R. Figure 4.13 is a snapshot of this visualization.

Figure 4.13 – Three dimensional rendering of the simulated channel system.
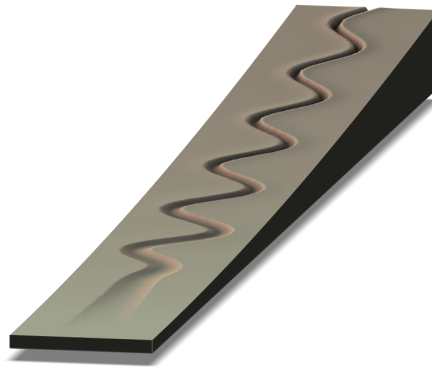
Source: Author

Furthermore, since the model is evolutive, the time tracking is also important for its understanding. Hence, animated GIFs were implemented representing the system evolution (Figure 4.14).

Figure 4.14 – Several frames (with corresponding timestamps) from a simulation illustrating a system's evolution.

t_0 t_1 t_2

t_3 t_4 t_5

t_6 t_7 t_8

t_9 t_{10} t_{11}
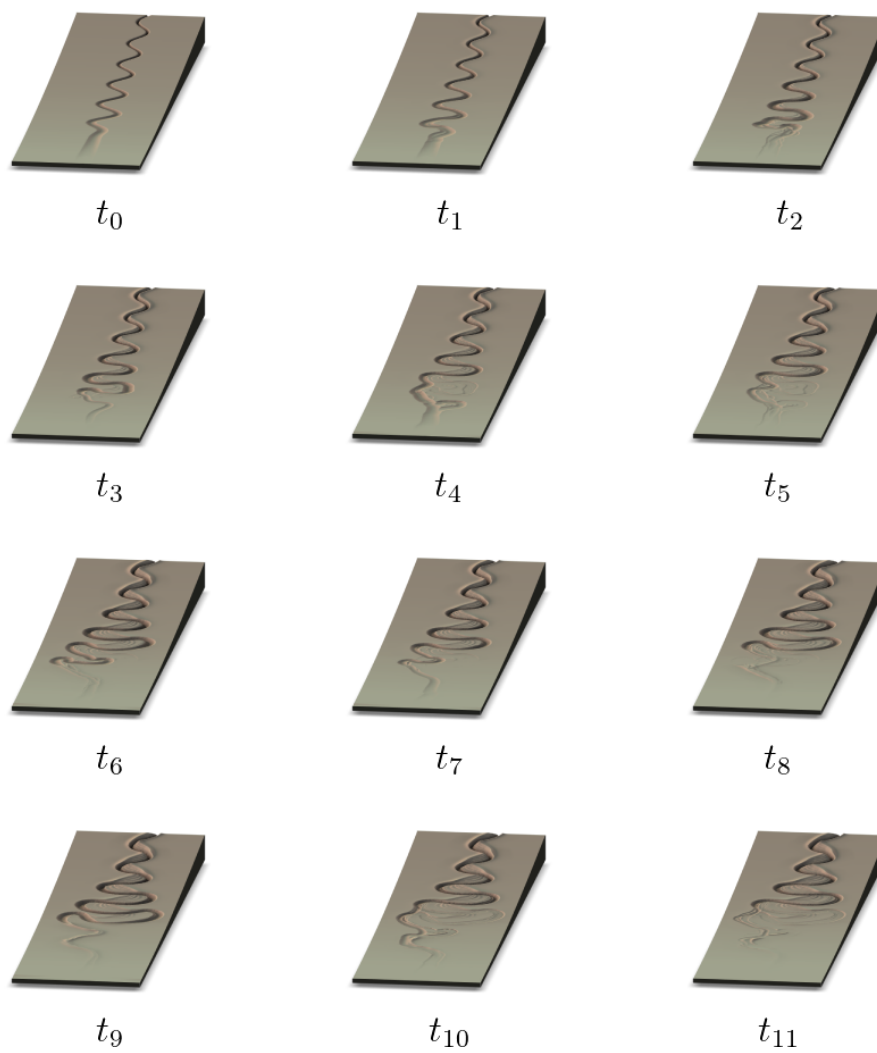
Source: Author

5 RESULTS AND VALIDATION

The present work was validated by geologists experts which confirms that method results reproduce similar system architectures found in nature, except for the lobes portions that do not emerge from this methodology. The lobules are a particular field of study and, in general, are modeled apart such as in (JO; PYRCZ, 2020) and (ABDELGAWAD et al., 2015). Besides, some illustrations in the literature can be used for comparison purposes.

The first comparison is based on the (MCHARGUE et al., 2011) work on which the architecture of turbidite systems is discussed. Figure 5.1 is part of the cited work and presents two different channel types formations that were used as inspiration for some simulations. However, the color scheme used in this image is different from the established in the presented methodology, thus, color matching is necessary. The yellow and grey colors represent the same deposit type in both schemes, sand, and pre-existing substrate. Green express mud-rich deposits which correspond to silt in our approach. The brown color represents mud-clast deposits that are fragments of rocks and can be associated with gravel in our description.

Figure 5.1 – Schematic representations of two channel elements. A: Under-filled channel with mud rich deposit. B: Filled channel with sand rich deposit.
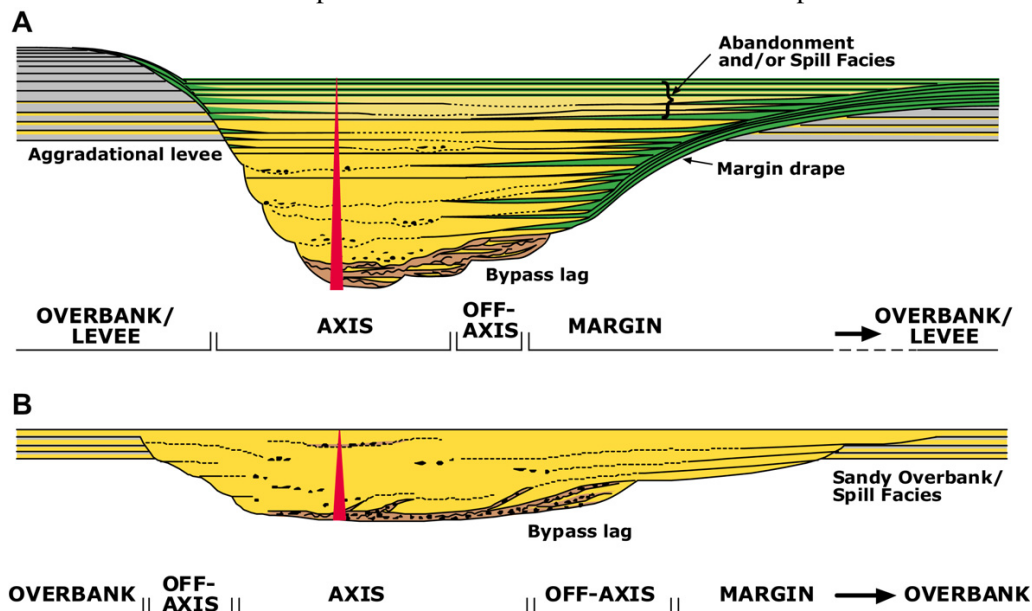
Source: (MCHARGUE et al., 2011)

Figure 5.2 was generated using one incision event and three aggradation events with different deposition and aggradation proportions. These events are shown in Appendix B. This image represents successfully the scenario in Figure 5.1-a.

Figure 5.2 – Cross-section image at $12.850\,\mathrm{km}$ reproducing similar architecture as in Figure 5.1-a.
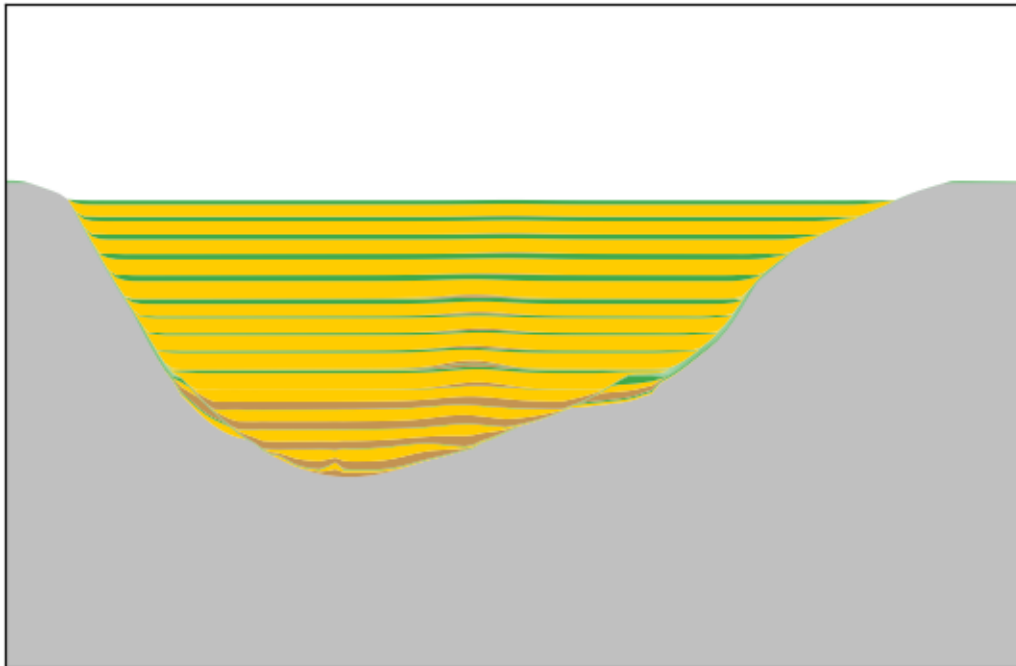
Source: Author

Figure 5.3 was created using one incision event and two aggradation events removing all silt material which are also presented in Appendix B - Listing 1. This image share important visual similarities with Figure 5.1-b.

Figure 5.3 – Cross-section image at $13.625\,\mathrm{km}$ reproducing similar architecture as in Figure 5.1-b.
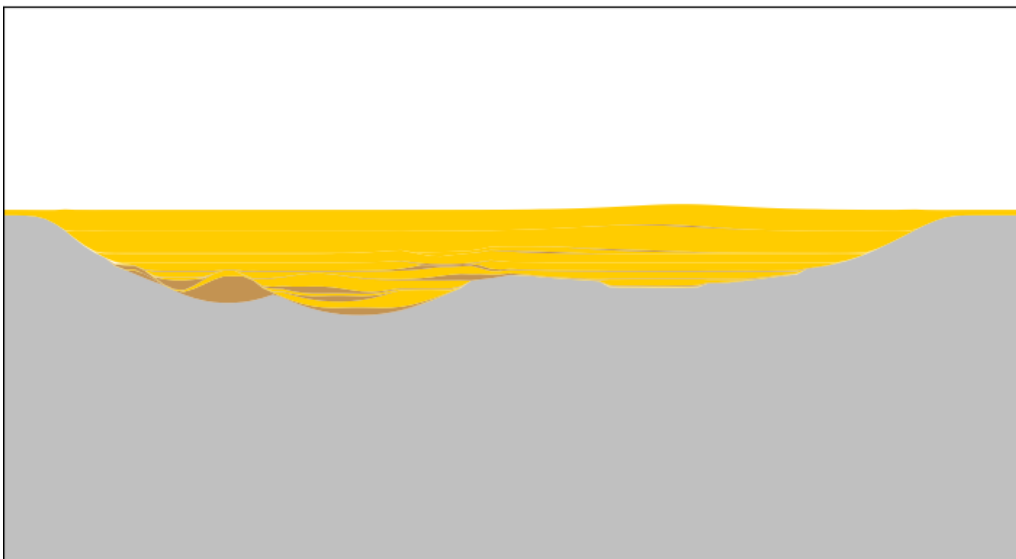
Source: Author

The (DEPTUCK et al., 2003) work was also used as the gold standard for comparison on which the architecture of channel systems in Africa. Figure W was adapted from

the cited work from a set of schematics snapshots of the filling evolution of such systems. The illustration is in greyscale, however, it is possible to identify three main deposits: substrate in light-grey, sand in normal grey, and gravel in dark grey. The silt deposits are not present in this representation but it is possible to interpret as the strongness of the black lines delimiting the deposits.
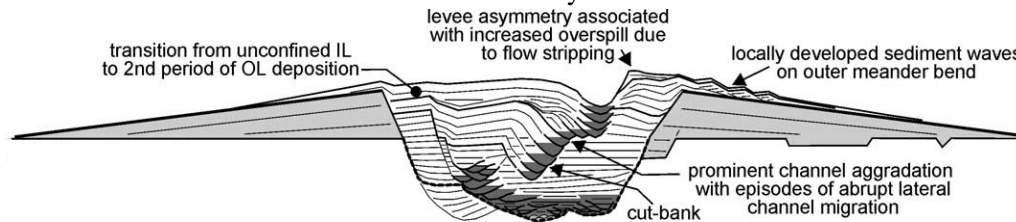
Figure 5.4 – Schematic drawing representing the channel filling phase of the Benin-major channel-levee system.

Source: adapted from (DEPTUCK et al., 2003)

Figure 5.5 is a cross-section image of a simulation using one incision event and three aggradation events. These aggradation events, however, have different aggradation factors reproducing periods of low and high aggradation which can be checked in Appendix B - Listing 2. This configuration produces similar architecture as shown in Figure 5.4, even though the substrate is always horizontal to the cross-section axis in this methodology.

Figure 5.5 – Cross-section image of an incision and long aggradation cycle simulation reproducing similar architecture as in Figure 5.4.
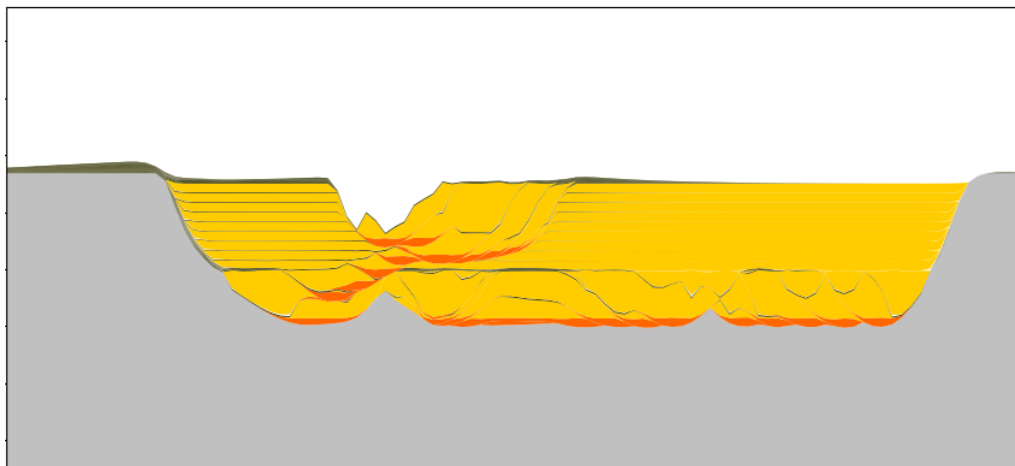
Source: Author

Besides the results shown in Figures 5.2, 5.3, and 5.5, we also simulated more complex system such those described in 2.1. Hence, we created two models containing a $20\,\mathrm{km}$ long channel in a basin that starts with a slope of $-5°$ and increases linearly until zero in the final part of the basin. Thus, the slope profile is a ramp, even though the terrain

profile is a parabolic arch, as shown in Figures 5.6 (Side View) and 5.9 (Side View). This configuration is similar to turbidite systems found in nature and also it is a good test case for our slope-driven simulation since we can verify different architectural formations along the channel evolution. In these simulations, we modeled 8 different events (with same time duration), four of which were incisions, and four were aggradation ones. The details of these events can be found in Appendix C - Listing 3 and 4. These events were defined in cycles of incision and aggradation containing different velocity factors simulating common behaviors of turbidite channel systems.

We refer to these two models as *Configuration I* and *Configuration II* since although they use different parameters, they share the initial basin, initial channel, and events. Table 5.1 presents the the set of distinct parameters used by each model. The resulting channel systems are shown in Figure 5.6 (3D View) and Figure 5.9 (3D View), respectively. It is important to note that the parameters dep_{props} and $aggr_{props}$ (as any other parameter in our simulator), shown in Table 5.1, could have been defined as functions of the slope s. However, in these two configurations they were considered independent of the slope and treated as constants for all events. The use of constant parameters like these is useful when simulating wide basins on which the turbidity currents do not contain enough power to carry the denser material all along the course.

Table 5.1 – Parameters used in two complete turbidite system simulations (Configuration I and II). ch_{depth} is the channel depth in meters, s is the local terrain slope in degrees, dep_{depth} is the deposition depth, dep_{props} are the deposition proportions of the material filling the deposion depth, $aggr_{props}$ are the proportions of the materials used in aggradation cycle, G stands for gravel, SA for sand, and SI for silt.

	ch_{depth} (m)	dep_{depth} (m)	dep_{props} $(G\%, SA\%, SI\%)$	$aggr_{props}$ $(G\%, SA\%, SI\%)$
Configuration I	$f(s) = -20s$	$f(s) = -5s$	(30%, 50%, 20%)	(33%, 33%, 33%)
Configuration II	$f(s) = 6s^2$	$f(s) = 4s^2$	(10%, 70%, 10%)	(10%, 70%, 10%)

Figure 5.7 shows the top view of the system corresponding to Configuration I, which has 4 cross-section locations indicated by the letters *A*, *B*, *C* and *D*. These cross sections were placed in equal spaced regions 20%, 40%, 60%, and 80% of the total basin length respectively, which are found in Figure 5.8.

The locations of these sections were chosen considering two goals: first, provide a comparison with the architecture schematics (Figure 2.2) of the turbidite channel systems developed by (SPRAGUE et al., 2002); and, second, represent four very different stages of a system. A description of each cross section is given below:

- Cross section A is at the beginning of the basin, where the slope is steep (approxi-

Figure 5.6 – Side and 3D view of the complete turbidite channel system with configuration I simulation.
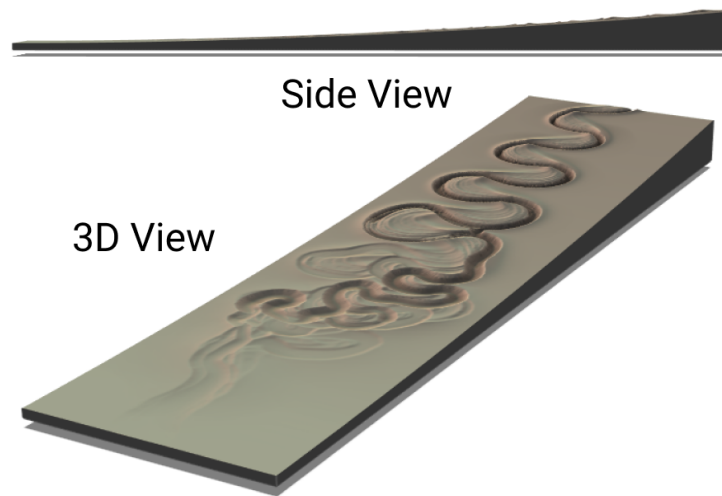
Source: Author

mately −4°) and corresponds to a *Canyon* with its V shape;

- Cross section B is almost at the middle of the basin with a moderate slope (approximately −3°). This cross section corresponds to *Confined Channels* with more U-shaped channels confined by the levee in the complex margin;

- Cross section C is a bit after the basin's middle containing a low slope (approximately −2°). This cross section corresponds to *Weakly Confined Channels* on which the levee tends to not stick to the margins and the channel's deposits are flatter;

- Cross section D is at the end of the channel, containing a very low slope (approximately −1°). This section corresponds to *Lobe* formations. Even though the simulation successfully deposits channels with almost no lateral migration, some other deposition patterns, such as the lobe fan shape are still not properly simulated by our current prototype. This is a subject for future work.

Similar observations apply to the system associated to Configuration II, whose cross-sections (Figure 5.10) are located at the same places as in Configuration I. However, as can be noticed in Figure 5.11, the formations and the deposits of this model are different from the ones in Configuration I, despite the similarity of these formations to the turbidite system architecture described in (SPRAGUE et al., 2002). Note that the system in Configuration II shows sandier deposits, which were obtained with the use of a larger

Figure 5.7 – Top view of the complete turbidite channel system simulation with Configuration I, delimiting 4 regions (A, B, C, and D) that represents different architecture formations.
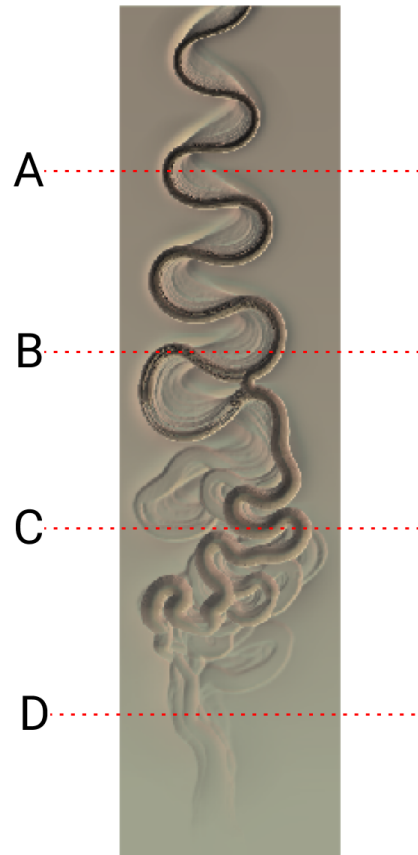
Source: Author

proportion of sand in the simulated events. The channels also tend to be shallower in Configuration II, mostly from the middle to the end of the basin. This behavior is explained by the different depth functions used in the description of the events, on which the quadratic parameterization used in Configuration II decays faster than the linear parameterizion used in Configuration I.

The execution times shown in Table 5.2 were measured on an *Intel® Core™ i5-8365U CPU @ 1.60GHz × 8 15.3 GiB RAM*. On this table, *Iterations* are the number of meandering steps ran in total for all events, *Layers* are the number of the saved steps on which the 3D model is generated, and the *Execution Time* is the approximated time in seconds spent simulating and also exporting the model. The difference in the execution time between Configuration I and II shows the non-linearity of the involved algorithms.

Figure 5.8 – Cross-sections views the complete turbidite channel system simulation with Configuration I, on which each image belongs to one region that is marked in Figure 5.7.
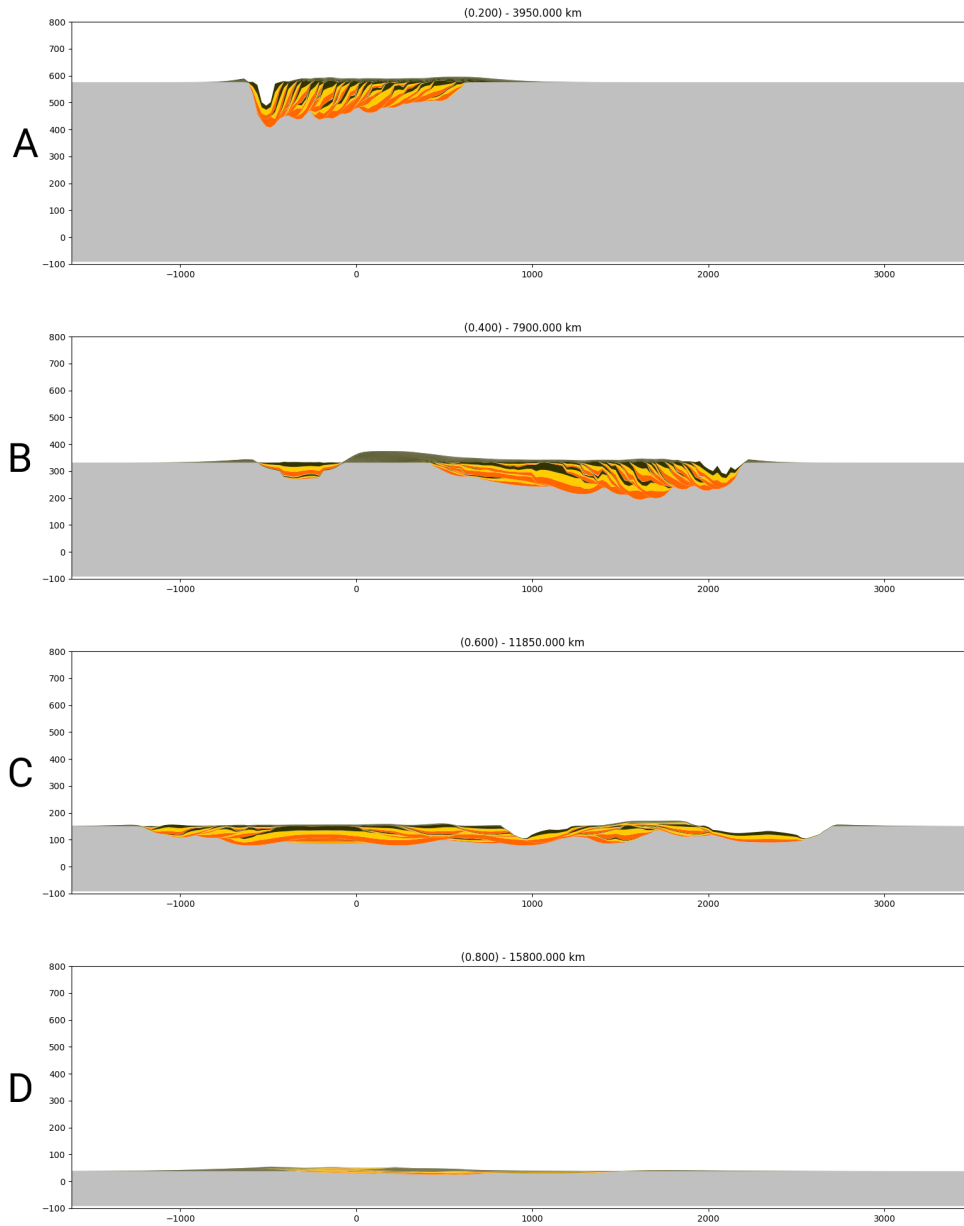
Source: Author

Even with the same number of iterations and layers, the different event relations leads to considerable difference in execution time.

Table 5.2 – Summary of the simulation process of the two complete turbidite system simulations (Configuration I and II).

	Iterations (#)	Layers(#)	Execution Time (s)
Configuration I	800	32	60 s
Configuration II	800	32	45 s

Figure 5.9 – Side and 3D view of the complete turbidite channel system with Configuration II simulation.

Source: Author

5.1 Summary

This chapter presented several results generated with our slope-driven channel simulation system. Some qualitative validation was performed by trying to reproduce some schematic cross sections found in the literature, as well as by evaluating the overall consistency of the channel architecture across the terrain slope variation.

Figure 5.10 – Top view of the complete turbidite channel system simulation with Configuration II, delimiting 4 regions (A, B, C, and D) that represents different architecture formations.
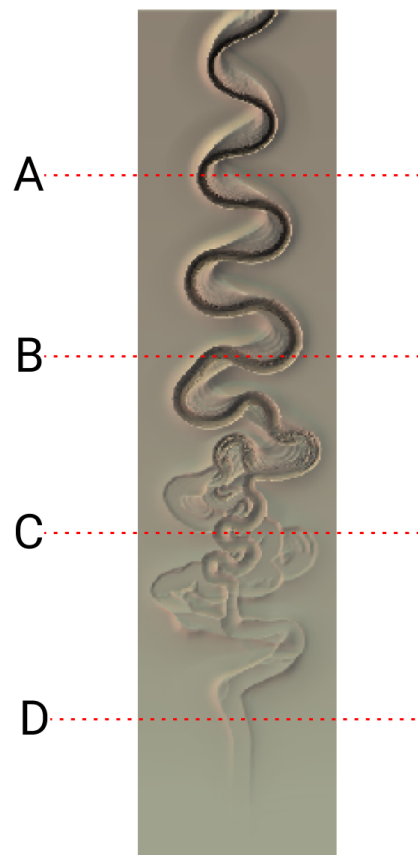
Source: Author

Figure 5.11 – Cross-sections views the complete turbidite channel system simulation with Configuration II, on which each image belongs to one region that is marked in Figure 5.10.
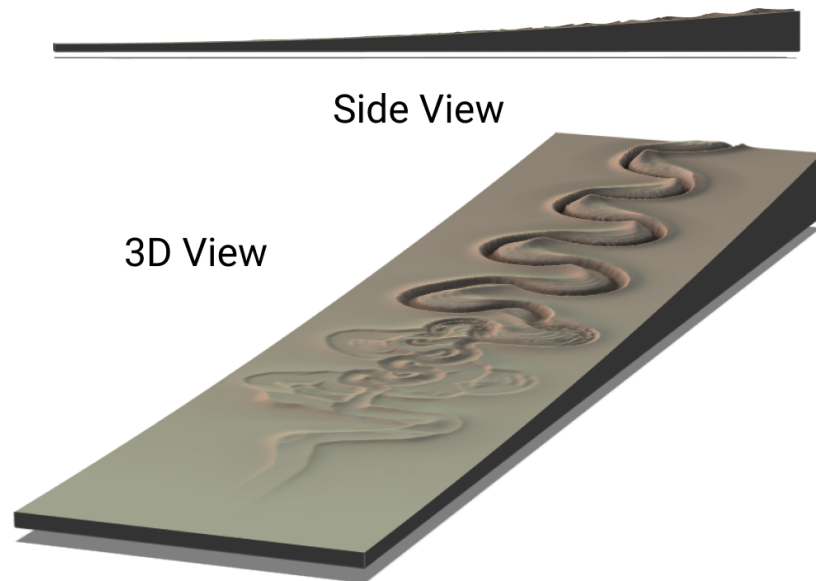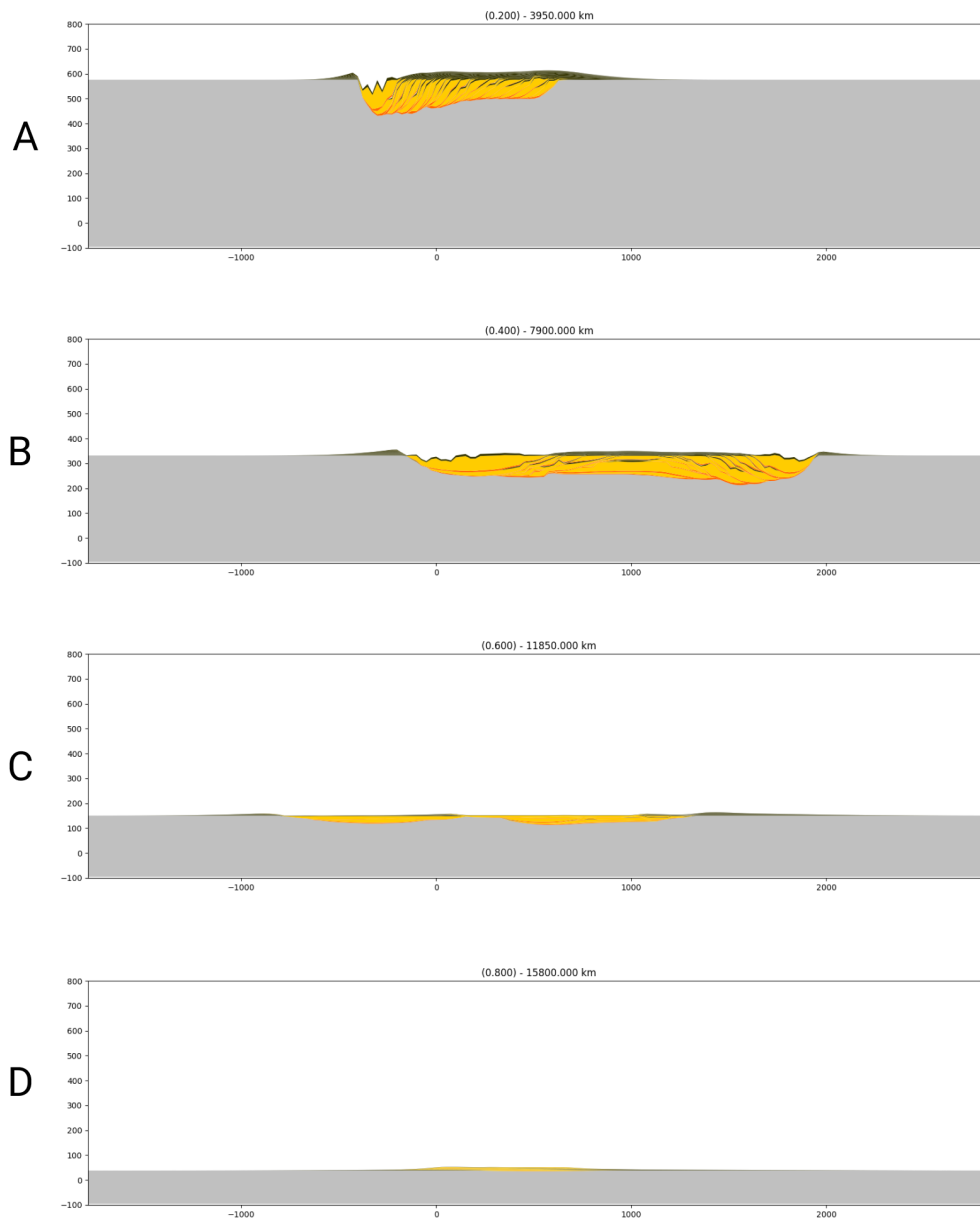

Source: Author

6 CONCLUSION AND FUTURE WORKS

The main goal of the proposed work was reached even though the lobule formations are not yet properly represented in the methodology. This approach can produce a large variety of models and still allow the control of the simulation overall behavior as was shown in Chapter 5 on which specific scenarios were modeled to match the formations described in the literature.

Moreover, the parametrization based on the slope has shown a great value and has enhanced the comprehensibility since the vast majority of the works in the area use the slope as a determinant factor for system architecture description. Hence, the parameters used for modeling are easily extracted from outcrop characterization data available in scientific papers and reports. Other than that, the events abstraction proposed in this work is quite straightforward and helpful for reservoir modelers since the system description requires hypotheses of how was the system development which is in general organized in a timeline of distinct system behavior. Besides, the event abstraction was specially designed for easy extensibility. Adding newer event types is simpler than creating new parameters to a single simulation method. Thus, our simulation pipeline can react to the specific event type instead of dealing with a set of parameters globally.

In order to continue the studies in this research area, some topics are listed below for further works:

- Cross-section images generation in any direction. As discussed previously, the cross-section images are only constructed parallel to the course axis of the simulation volume. However, this limitation may impact the data interpretation since some formations can be hidden in planes that can not be represented;

- Integration of a hierarchical model for depositional lobes. The lobes formations have their particular stacking pattern which requires specific treatment;

- Implementation of a user interface. The current package hard codes some of the inputs and simulation parameters. Hence, a graphical interface would enhance the modelers' experience;

- Implementation of an interactive visualization module. Channel evolution over time is also an important aspect for our simulator. In the current prototype, animated GIF videos were used to demonstrate this. A visualization module that supports interactive exploration of the 3D channel system, time-slice selection, as well animated views of channel evolution should significantly enhances the potential of our system

in helping geologists to understand tubidite channel systems.

REFERENCES

ABDELGAWAD, S. et al. **A Novel Approach for Modeling Deepwater Turbidite Lobes**. Doha, Qatar: International Petroleum Technology Conference, 2015. 7 p. IPTC. Available from Internet: <https://doi.org/10.2523/IPTC-18292-MS>.

AG2GAEH. **Two definitions of a parallel curve: 1) envelope of a family of congruent circles, 2) by a fixed normal distance**. 2015. Online; accessed 03-03-2021. Available from Internet: <https://commons.wikimedia.org/wiki/File:Offset-definition-poss.svg>.

COVAULT, J. Submarine fans and canyon-channel systems: A review of processes, products, and models. **Nature Education Knowledge**, v. 3, p. 4, 01 2011.

DEPTUCK, M. et al. Migration–aggradation history and 3-d seismic geomorphology of submarine channels in the pleistocene benin-major canyon, western niger delta slope. **Marine and Petroleum Geology**, v. 24, p. 406–433, 06 2007.

DEPTUCK, M. E. et al. Architecture and evolution of upper fan channel-belts on the niger delta slope and in the arabian sea. **Marine and Petroleum Geology**, v. 20, n. 6, p. 649–676, 2003. ISSN 0264-8172. Turbidites: Models and Problems. Available from Internet: <https://www.sciencedirect.com/science/article/pii/S0264817203001235>.

EMPERORHONEY. **Curvature is a computed characteristic of a curve (or surface) at a point. Curvature uses the notion of the "osculating circle" of radius R at Point P.** 2020. Online; accessed 17-02-2021. Available from Internet: <https://commons.wikimedia.org/wiki/File:Osculating.svg>.

HEEREMA, C. J. et al. What determines the downstream evolution of turbidity currents? **Earth and Planetary Science Letters**, v. 532, p. 116023, 2020. ISSN 0012-821X. Available from Internet: <https://www.sciencedirect.com/science/article/pii/S0012821X19307150>.

HIL, G. **BETTER MANAGEMENT THROUGH MEASUREMENT: Assessing the conditions of coastal archaeological sites using spatial technologies-applied to Blueskin Bay, New Zealand**. Thesis (PhD), 04 2018.

HOWARD, A.; KNUTSON, T. Sufficient conditions for river meandering: A simulation approach. **Water Resources Research**, v. 20, p. 1659–1667, 11 1984.

JO, H.; PYRCZ, M. J. Robust rule-based aggradational lobe reservoir models. **Natural Resources Research**, v. 29, n. 2, p. 1193–1213, Apr 2020. ISSN 1573-8981. Available from Internet: <https://doi.org/10.1007/s11053-019-09482-9>.

KNELLER, B. The influence of flow parameters on turbidite slope channel architecture. **Marine and Petroleum Geology**, v. 20, n. 6, p. 901–910, 2003. ISSN 0264-8172. Turbidites: Models and Problems. Available from Internet: <https://www.sciencedirect.com/science/article/pii/S0264817203001181>.

MCHARGUE, T. et al. Architecture of turbidite channel systems on the continental slope: Patterns and predictions. **Marine and Petroleum Geology**, v. 28, n. 3, p. 728–743, 2011. ISSN 0264-8172. Thematic Set on STRATIGRAPHIC EVOLUTION OF DEEP-WATER ARCHITECTURE. Available from Internet: <https://www.sciencedirect.com/science/article/pii/S0264817210001443>.

PATRIKALAKIS, N. Offsets of parametric curves and surfaces. 01 2003.

SMITS, A. J. **Continuity Equation**. 1997. Online; accessed 19-02-2021. Available from Internet: <https://www.princeton.edu/~asmits/Bicycle_web/continuity.html>.

SPRAGUE, A. et al. The physical stratigraphy of deep-water strata: A hierarchical approach to the analysis of genetically related stratigraphic elements for improved reservoir prediction. **AAPG Annual Convention Abstract**, p. 10–13, 01 2002.

SURFACE Water. 2020. Online; accessed 16-02-2021. Available from Internet: <https://geo.libretexts.org/Courses/Gettysburg_College/Book%3A_An_Introduction_to_Geology_(Johnson_Affolter_Inkenbrandt_and_Mosher)/09%3A_Water/9.07%3A_Surface_Water>.

SYLVESTER, Z. **Meanderpy**. 2019. [Software package; Online; acessado em julho de 2020]. Available from Internet: <https://github.com/zsylvester/meanderpy>.

SYLVESTER, Z.; PIRMEZ, C.; CANTELLI, A. A model of submarine channel-levee evolution based on channel trajectories: Implications for stratigraphic architecture. **Marine and Petroleum Geology**, v. 28, n. 3, p. 716 – 727, 2011. ISSN 0264-8172. Thematic Set on STRATIGRAPHIC EVOLUTION OF DEEP-WATER ARCHITECTURE. Available from Internet: <http://www.sciencedirect.com/science/article/pii/S0264817210001157>.

WANG, Y. **RULE-BASED RESERVOIR MODELING BY INTEGRATION OF MULTIPLE INFORMATION SOURCES: LEARNING TIME-VARYING GEOLOGIC PROCESSES**. Dissertation (Master) — STANFORD UNIVERSITY, 2015.

WANG, Z. et al. **River Morphodynamics and Stream Ecology of the Qinghai-Tibet Plateau**. [S.l.: s.n.], 2016. ISBN 9781138027718.

WEIMER, P.; PERKINS, B. F. Deep-water reservoirs of the world : Gulf coast section society of economic paleontologists and mineralogists foundation, 20th annual bob f. perkins research conference, december 3-6, 2000, houston, texas. In: . Houston : GCSSEPM : produced by The Write Enterprise, 2000., 2000. Available from Internet: <https://search.library.wisc.edu/catalog/999913073402121>.

ZHANG, L.-F.; PAN, M.; LI, Z.-L. 3d modeling of deepwater turbidite lobes: a review of the research status and progress. **Petroleum Science**, v. 17, n. 2, p. 317–333, Apr 2020. ISSN 1995-8226. Available from Internet: <https://doi.org/10.1007/s12182-019-00415-y>.

Appendices

Appendix A PLOTTED RELATIONS

In Figure A.1 is shown a plotted that is available in the our package for summarize and visualize all relations presented in a event.

Figure A.1 – The default relations used for channel parameters, computed based on the terrain slope. From left to right, top to bottom: depth, width, deposition height, deposition proportions, deposition standard deviation (sigma), aggradation proportions, aggradation standard deviation (sigma).
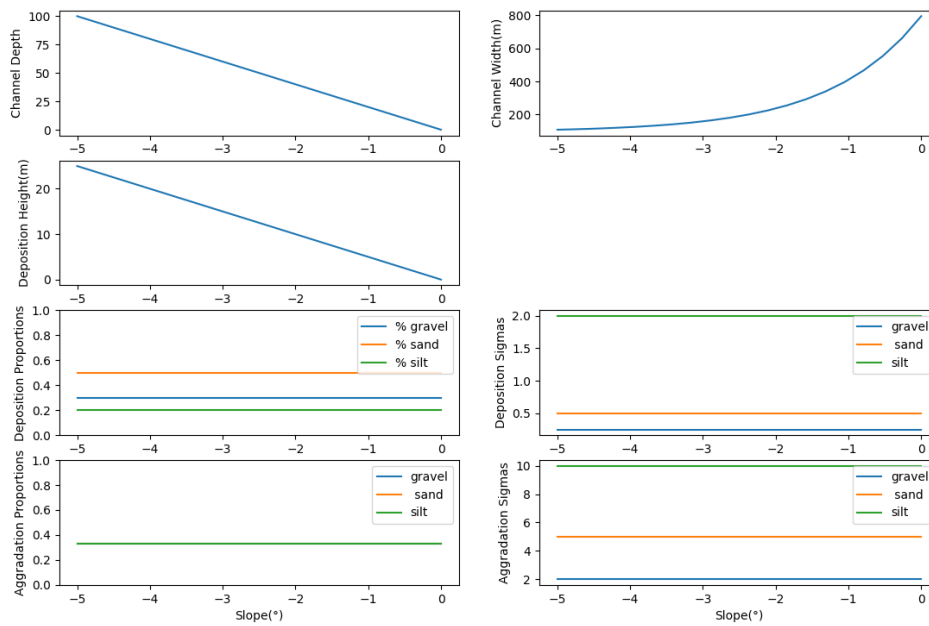
Source: Author

Appendix B VALIDATION CODE

In Listings 1 and 2 are presented the code used for generating the models similar to those in literature.

```python
events_a = [
  mp.ChannelEvent(nit = 150, saved_ts = 25, Cf = 0.02,
  ↪  mode='INCISION', kv = 0.0033 * 12, dep_props=lambda x: (0,
  ↪  0.85, 0.15)),
  mp.ChannelEvent(nit = 50, saved_ts = 10, Cf = 0.02,
  ↪  mode='AGGRADATION', aggr_factor=1, kv = 0.0033 * 15,
  ↪  aggr_props=lambda x: (0.4, 0.6, 0.0), dep_props= lambda x:
  ↪  (0.6, 0.3, 0.1)),
  mp.ChannelEvent(nit = 50, saved_ts = 10, Cf = 0.02,
  ↪  mode='AGGRADATION', aggr_factor=1, kv = 0.0033 * 15,
  ↪  aggr_props=lambda x: (0, 0.9, 0.1), dep_props= lambda x: (0.8,
  ↪  0.0, 0.2)),
  mp.ChannelEvent(nit = 100, saved_ts = 15, Cf = 0.02,
  ↪  mode='AGGRADATION', aggr_factor=1, kv = 0.0033 * 15,
  ↪  aggr_props=lambda x: (0, 0.75, 0.25), dep_props= lambda x:
  ↪  (0.8, 0.0, 0.2)),
]

events_b = [
  mp.ChannelEvent(nit = 150, saved_ts = 25, Cf = 0.02,
  ↪  mode='INCISION', kv = 0.0033 * 5, aggr_props=lambda x: (0.8,
  ↪  0.2, 0), dep_props= lambda x: (0.8, 0.2, 0)),
  mp.ChannelEvent(nit = 50, saved_ts = 10, Cf = 0.02,
  ↪  mode='AGGRADATION', aggr_factor=2, kv = 0.002 * 5,
  ↪  aggr_props=lambda x: (0.1, 0.9, 0), dep_props= lambda x: (0.8,
  ↪  0.2, 0)),
  mp.ChannelEvent(nit = 100, saved_ts = 25, Cf = 0.02,
  ↪  mode='AGGRADATION', aggr_factor=2, kv = 0.002 * 5,
  ↪  aggr_props=lambda x: (0, 1, 0), dep_props= lambda x: (0.25,
  ↪  0.75, 0.0)),
]
```

Listing 1 – Definition code for the events used to reproduce the similar (MCHARGUE et al., 2011) system.

```python
events = [
  mp.ChannelEvent(nit = 100, saved_ts = 25, Cf = 0.02,
  ↪   mode='INCISION', kv = 0.0033 * 10, dep_props= lambda x: (0.9,
  ↪   0, 0.1), aggr_props= lambda x: (0, 1, 0)),
  mp.ChannelEvent(nit = 150, saved_ts = 25, Cf = 0.02,
  ↪   mode='AGGRADATION', kv = 0, dep_props= lambda x: (0.9, 0, 0.1),
  ↪   aggr_props= lambda x: (0, 1, 0)),
  mp.ChannelEvent(nit = 150, saved_ts = 15, Cf = 0.02,
  ↪   mode='AGGRADATION', aggr_factor=2, kv = 0.0033 * 5, dep_props=
  ↪   lambda x: (0.9, 0, 0.1), aggr_props= lambda x: (0, 1, 0)),
  mp.ChannelEvent(nit = 150, saved_ts = 15, Cf = 0.02,
  ↪   mode='AGGRADATION', kv = 0, dep_props= lambda x: (0.9, 0, 0.1),
  ↪   aggr_props= lambda x: (0, 1, 0)),
]
```

Listing 2 – Definition code for the events used to reproduce the similar (DEPTUCK et al., 2003) system.

Appendix C COMPLETE SYSTEM CODE

In Listings 3 and 4 are shown the code of events used to simulate complete turbidite system with configuration I and II, respectively.

```
events = [
    mp.ChannelEvent(nit = 100, saved_ts = 25, mode='INCISION', kv =
    ↪  0.0033 / ONE_YEAR),
    mp.ChannelEvent(nit = 100, saved_ts = 25, mode='AGGREGATION',
    ↪  aggr_factor=2, kv = 0.002 / ONE_YEAR),
    mp.ChannelEvent(nit = 100, saved_ts = 25, mode='INCISION', kv =
    ↪  0.0033 / ONE_YEAR),
    mp.ChannelEvent(nit = 100, saved_ts = 25, mode='AGGREGATION',
    ↪  aggr_factor=2, kv = 0.002 / ONE_YEAR),
    mp.ChannelEvent(nit = 100, saved_ts = 25, mode='INCISION', kv =
    ↪  0.002 / ONE_YEAR),
    mp.ChannelEvent(nit = 100, saved_ts = 25, mode='AGGREGATION',
    ↪  aggr_factor=2, kv = 0.0033 / ONE_YEAR),
    mp.ChannelEvent(nit = 100, saved_ts = 25, mode='INCISION', kv =
    ↪  0.002 / ONE_YEAR),
    mp.ChannelEvent(nit = 100, saved_ts = 25, mode='AGGREGATION',
    ↪  aggr_factor=2, kv = 0.0033 / ONE_YEAR)
]
```

Listing 3 – Definition code for the events used to simulate the complete turbidite system with configuration I.

```python
ch_depth = lambda slope: 6 * slope ** 2
dep_height = lambda slope: 4 * slope ** 2
dep_props = lambda slope: (0.1, 0.8, 0.1)
aggr_props = lambda slope: (0.1, 0.8, 0.1)
events = [
    mp.ChannelEvent(nit = 100, saved_ts = 25, mode='INCISION',
    ↪  ch_depth = ch_depth, dep_height = dep_height, dep_props =
    ↪  dep_props, aggr_props = aggr_props, kv = 0.0033 / ONE_YEAR),
    mp.ChannelEvent(nit = 100, saved_ts = 25, mode='AGGREGATION',
    ↪  ch_depth = ch_depth, dep_height = dep_height, dep_props =
    ↪  dep_props, aggr_props = aggr_props, aggr_factor=2, kv = 0.002
    ↪  / ONE_YEAR),
    mp.ChannelEvent(nit = 100, saved_ts = 25, mode='INCISION',
    ↪  ch_depth = ch_depth, dep_height = dep_height, dep_props =
    ↪  dep_props, aggr_props = aggr_props, kv = 0.0033 / ONE_YEAR),
    mp.ChannelEvent(nit = 100, saved_ts = 25, mode='AGGREGATION',
    ↪  ch_depth = ch_depth, dep_height = dep_height, dep_props =
    ↪  dep_props, aggr_props = aggr_props, aggr_factor=2, kv = 0.002
    ↪  / ONE_YEAR),
    mp.ChannelEvent(nit = 100, saved_ts = 25, mode='INCISION',
    ↪  ch_depth = ch_depth, dep_height = dep_height, dep_props =
    ↪  dep_props, aggr_props = aggr_props, kv = 0.002 / ONE_YEAR),
    mp.ChannelEvent(nit = 100, saved_ts = 25, mode='AGGREGATION',
    ↪  ch_depth = ch_depth, dep_height = dep_height, dep_props =
    ↪  dep_props, aggr_props = aggr_props, aggr_factor=2, kv =
    ↪  0.0033 / ONE_YEAR),
    mp.ChannelEvent(nit = 100, saved_ts = 25, mode='INCISION',
    ↪  ch_depth = ch_depth, dep_height = dep_height, dep_props =
    ↪  dep_props, aggr_props = aggr_props, kv = 0.002 / ONE_YEAR),
    mp.ChannelEvent(nit = 100, saved_ts = 25, mode='AGGREGATION',
    ↪  ch_depth = ch_depth, dep_height = dep_height, dep_props =
    ↪  dep_props, aggr_props = aggr_props, aggr_factor=2, kv =
    ↪  0.0033 / ONE_YEAR)
]
```

Listing 4 – Definition code for the events used to simulate the complete turbidite system with configuration II